HHS Public Access

Author manuscript

Biomater Sci. Author manuscript; available in PMC 2023 May 17.

Published in final edited form as:

Biomater Sci. ; 10(10): 2590–2608. doi:10.1039/d1bm01890f.

Hyaluronan and Elastin-Like Protein (HELP) Gels Significantly Improve Microsphere Retention in the Myocardium

Riley A. Suhar[a], **Vanessa M. Doulames**[a,b], **Yueming Liu**[a], **Meghan E. Hefferon**[a,b], **Oscar Figueroa III**[c], **Hana Buabbas**[a,d], **Sarah C. Heilshorn**[a,*]

[a]Department of Materials Science and Engineering, Stanford University, Stanford, California 94305, USA

[b]Department of Neurosurgery, Stanford University School of Medicine, Stanford, California 94305, United States

[c]Unaffiliated

[d]Department of Biology, Stanford University, Stanford, California, 94305, United States

Abstract

Heart disease is the leading cause of death globally, and delivery of therapeutic cargo (*e.g.,* particles loaded with proteins, drugs, cells, or genes) through direct injection into the myocardium is a promising clinical intervention. However, retention of deliverables to the contracting myocardium is low, with as much as 60 – 90% of payload being lost within 24 hours. Commercially-available injectable hydrogels, including Matrigel, have been hypothesized to increase payload retention, but have not yielded significant improvements in quantified analyses. Here, we assess a recombinant hydrogel composed of chemically modified hyaluronan and elastin-like protein (HELP) as an alternative injectable carrier to increase cargo retention. HELP is crosslinked using dynamic covalent bonds, and tuning the hyaluronan chemistry significantly alters hydrogel mechanical properties including stiffness, stress-relaxation rate, and ease of injectability through a needle or catheter. These materials can be injected even after complete crosslinking, extending the time window for surgical delivery. We show that HELP gels significantly improve *in vivo* retention of microsphere cargo compared to Matrigel, both 1 day and 7 days post-injection directly into the rat myocardium. These data suggest that HELP gels may assist with the clinical translation of therapeutic cargo designed for delivery into the contracting myocardium by preventing acute cargo loss.

[*]Corresponding author. heilshorn@stanford.edu (S.C.H.), Address: 476 Lomita Mall, McCullough Room 246, Stanford University, Stanford, CA, 94305-4045, USA, Fax Number: 650-723-3044.

6. CRediT Author Statement

Riley A. Suhar: Conceptualization, Investigation, formal analysis, resources, writing – original draft, data curation, visualization, project administration, resident rockstar; **Vanessa M. Doulames:** Investigation, formal analysis, resources, writing – review & editing; **Yueming Liu:** Investigation, data curation; **Meghan E. Hefferon**: Investigation, resources; **Oscar Figueroa III**: Software, validation; **Hana Buabbas:** Resources; **Sarah C. Heilshorn:** Conceptualization, writing – review & editing, supervision, funding acquisition.

Keywords

Cardiovascular Disease; Myocardial Infarction; Hydrogel; Elastin-Like Protein; Hyaluronic Acid; Protein Engineering

1. Introduction

The Global Burden of Disease Study in 2017 found that 31.8% of all deaths worldwide were from cardiovascular disease, over half of which were the direct result of ischemic heart disease [1]. Since the 1960's, the short-term (< 1 year) survival rate following a myocardial infarction (MI) has increased world-wide [2–4]. Despite these improvements, mortality from end-stage heart failure (HF) following MI is still very high, with 13% of patients being diagnosed with HF within 30 days of the initial infarction and 20–30% within the first year [5,6]. Surgical interventions such as cardiac restraints have been shown to be insufficient at limiting HF [7,8], and heart transplants are an unsustainable practice because of severe organ shortages [8,9]. Direct injection of therapeutic agents into the myocardium to prevent HF can be surgically accomplished through noninvasive catheterization, making this strategy an attractive clinical option. To this end, the regenerative potential of a multitude of therapies have been studied as a means to improve cardiac function and prevent HF. In particular, microspheres loaded with various bioactive compounds, including cells [10–12], gene therapy [13,14], proteins [15,16], drugs [17], and exosomes [18], have gained considerable interest. However, many of these therapies, which typically use saline or aqueous medium as a carrier, are severely limited because of their low retention within the contracting myocardium (Figure 1A) [10,12,19–22]. While direct quantification of microsphere retention is rare in the literature, data on acute retention of cell therapies highlights the challenges of delivery within a mechanically active tissue. For example, a clinical trial studying the distribution of radio-labeled bone marrow cells injected directly into the myocardium with a liquid medium carrier found that within 1 hour as much as ~90% of cells had been ejected [23]. Other human and animal trials studying cargo retention have shown similar results [24–27]. As cargo retention has been correlated with cardiac function and repair [28,29], it is vital that we develop systems which improve retention post-injection.

It is commonly hypothesized that injectable hydrogels may be able to increase cargo retention by physically anchoring the injected cargo within the delivery site and resisting mechanical expulsion [30,31]. However, retention of therapeutic agents is highly variable between studies, in part due to variations in quantification methods and surgical technique [32]. Additionally, there are very few head-to-head studies comparing retention rates of different hydrogel carriers, which makes direct comparisons particularly difficult. One study showed that the use of commercially available hydrogels (either Matrigel or Pluronic F127) showed qualitative reduction in acute expulsion of fluorescent microspheres compared with saline, but the differences were not statistically significant [30]. Interestingly, microsphere retention did not significantly change between the acute phase (10 minutes) and later time points (1 week), suggesting that the majority of cargo loss occurred at the time of injection and shortly thereafter. These findings correlate with clinical observations, which highlight

the importance of improving retention at the time of injection [23–27]. Mechanical beating of the heart and evacuation, either through ruptured blood vessels or the needle tract, have been identified as key modes of acute cargo loss [27,33]. In response, some have posited that hydrogels with more robust mechanics may better resist these mechanical challenges and therefore improve acute retention [30,34].

We have recently developed a two-part, hyaluronan and elastin-like protein (HELP) hydrogel system (Figure 1B) that is injectable, cell-compatible, and has independently tunable mechanical and biochemical properties [35–37]. Briefly, the hyaluronan (also termed hyaluronic acid, HA) component can be functionalized either through oxidation or conjugation chemistry to have a pendant aldehyde moiety. The elastin-like protein (ELP) is a recombinantly derived protein that contains (I) a bio-active region with a human fibronectin-derived, cell-adhesive, extended RGD sequence and (II) an elastin-like region that includes multiple lysine residues (Figure S1). The lysine residues are functionalized with a hydrazine moiety, which form hydrazone bonds when mixed with aldehyde groups to spontaneously form a dynamic covalently crosslinked polymer network. Here, we expand upon our previously reported system by formulating five different HELP variants with distinct material properties to identify underlying material design rules that significantly improve cargo delivery to and retention within the contractile myocardium. In particular, we demonstrate that by careful tuning of the HA component, we can significantly alter the matrix stiffness, stress-relaxation rate, and ease of injectability of HELP hydrogels through needles and catheters. We further show that HELP gels significantly increase the retention of fluorescent microspheres in the contracting myocardium *in vivo* compared to Matrigel. These data suggest that HELP gels may assist with the clinical translation of therapeutic cargo designed for delivery into the contracting myocardium by preventing acute cargo loss.

2. Materials and Methods

2.1 Expression of Elastin Like Protein:

Our elastin-like proteins (ELP) are expressed in BL21 (DE3) pLysS *Escherichia coli* (Invitrogen, 1931008) under control of the T7 promoter, as previously described [38]. Briefly, an ELP plasmid containing stock is streaked across a co- ampicillin and chloramphenicol infused and incubated over-night at 37 °C. The following morning, a single colony is selected and used to inoculate a starter culture with ampicillin, and grown overnight at 37°C under constant agitation. 20 mL of starter culture is subsequently dispersed into 12, 1L baffled flasks and at 37 °C to an optical density (λ = 600 nm) of 0.8. Expression is induced by addition of 1 mM Isopropyl β-d-1-thiogalactopyranoside (IPTG; Thermo, BP1755–100). After 7 hours of expression at 32 °C, ELP-containing *E. coli* cells are collected by centrifugation, re-suspended in TEN buffer (0.1 M Tris-Cl, 0.01 M EDTA, 1 M NaCl, pH 8.0) and then frozen at −80 °C.

The *E. coli* cells are lysed via repeated freeze-thaw cycles. 1 mM phenylmethylsulfonyl fluoride (PMSF; ThermoScientific, 36978) and ~ 30 mg deoxyribonuclease I (Sigma, DN25) is added after the first cycle. After the completion of the freeze-thaw cycles, the ELP-lysate mixture is cooled to 4°C and then centrifuged at ≥ 15,000 × g at 4 °C for 1 hour. The supernatant is then incubated at 37°C for 4 hours under constant agitation. Precipitation is

further assisted by the addition 0.1 M NaCl. Combined, this induces the LCST behavior which results in a two-phase mixture of un-solubilized ELP and solution. The resulting mixture is centrifuged at ≥ 15,000 × g, 37 °C, for 1 hour and the ELP-rich pellet is then manually broken up with a small spatula to assist in re-solubilization. The mashed pellet is then mixed with ultra-pure distilled (DI) water (10 mL g^{-1}) and mixed overnight on an orbital shaker at 4 °C. This thermal cycling procedure is repeated a total of 3 times. The resulting solution is dialyzed against 4 L of DI water at 4°. The 4-L of dialysis water is routinely refreshed every 12 hours over the course of 3 days. The dialyzed product is then sterilized using a 0.22-μm syringe filter, frozen, and lyophilized for 3 days.

2.2 Functionalization of Elastin-Like Protein with Hydrazine:

The ELP used presently contains a central lysine (K) group within the elastin-like region. These lysine moieties were functionalized with hydrazine groups according to the following protocol [35,37]. First, ELP wass dissolved in anhydrous dimethyl sulfoxide (DMSO) at 6% (w/v). Following complete dissolution of the ELP, an equal volume of N,N-dimethylformamide (DMF) was added to the reaction mixture. In a separate round-bottom flask: (1) tri-Boc-hydrazinoacetic acid (Tri-Boc; 2 equiv:ELP amine (14 total amine/ELP); ChemImpex, 16931), (2) hexafluorophosphate azabenzotriazole tetramethyl uronium (HATU; 2 equiv:ELP amine, Sigma, 445460), and (3) 4-methylmorpholine (4.5 equiv:ELP amine; Sigma, M56557) were dissolved in DMF at room temperature (RT) to allow for the activation of free acid groups on the Tri-Boc molecule by HATU. The reagent solution is added, dropwise, to the ELP resulting in a final ELP concentration of 2% (w/v). The reaction was carried out overnight at RT under constant agitation.

The reaction solution was then added dropwise into ice-cold diethyl ether to a final volumetric ratio of 1:5 (reaction volume:ether). Modified ELP was collected by centrifugation (>18000 × g) at 4 °C for 30 minutes, decanted, and dried over-night yielding a Boc-protected intermediate. A small sample (~10 mg) was collected for downstream analysis of functionalization efficiency via NMR (below). To remove the Boc protecting groups, the ELP-hydrazine intermediate was dissolved at 2% (w/v) in a 1:1 mixture of Dichloromethane and trifluoroacetic acid with 2.5% v/v tri-isopropylsilane (Sigma, 233781) and stirred at RT for 4 hours. The de-protected product (ELP-Hydrazine) was then precipitated in chilled diethyl ether and centrifuged as described above. The final product was then dissolved in DI water at 2% (w/v) and dialyzed against 4-L of DI. The 4-L of dialysis water is routinely refreshed every 12 hours over the course of 3 days. The final dialyzed product is then sterilized using a 0.22-μm syringe filter, frozen, and finally lyophilized for 3 days in a sterile, filtered 50 mL tube (Millipore, SCGP00525).

2.3 Functionalization of Hyaluronic Acid with Aldehyde and Benzaldehyde Moieties via Copper-Click Reaction:

Hyaluronan (HA) was functionalized with either a aldehyde (HA-A) or benzaldehyde (HA-B) groups via copper-click chemistry is achieved with a two-part reaction. First, commercially available 100 kDa HA (Lifecore) was functionalized via EDC chemistry with alkyne groups. Second, a commercial small molecule with either a pendant benzaldehyde

group or a pendant aldehyde group is used to functionalize the alkyne groups via standard copper-click chemistry.

The procedure for alkyne modification has been described elsewhere [37]. Briefly, 100 kDa HA (sodium salt) was dissolved in MES buffer (0.2 M MES hydrate, 0.15 M NaCl in DI water; pH 4.5) at a concentration of 1% (w/v). Once dissolved, sufficient propargylamine (0.8 molar equivalent; Sigma Aldrich, P50900–5G) to functionalize 12% of the available carboxylic acid groups was added directly, and immediately following the pH was adjusted to 6.0 with 1M NaOH. N-hydroxysuccinimide (NHS; 0.8 molar equivalent) and 1-(3-dimethylaminopropyl)-3-ethylcarbodiimide hydrochloride (EDC; 0.8 molar equivalent) were added sequentially and allowed to react for 4 hours at RT with constant agitation. The reaction was then dialyzed against 4-L of DI water. The 4-L of dialysis water was routinely refreshed every 12 hours over the course of 3 days. The final dialyzed product was then sterile filtered using a 0.22-μm syringe filter, frozen, and finally lyophilized for 3 days, yielding HA-Alkyne.

Pendant aldehyde or benzaldehyde groups were attached to HA-Alkyne via standard copper-click chemistry to yield HA-A and HA-B, respectively. Briefly, HA-Alkyne was dissolved at 2.5% (w/v) in 10X isotonic phosphate buffered saline (10X PBS) with 0.85 mg mL^{-1} beta-cyclodextran supplement. After complete dissolution, the reaction mixture was degassed. 2.4 mM copper sulfate and 45.2 mM sodium ascorbate solutions were additionally prepared and degassed to remove excess oxygen. Depending on the intended modification scheme, a 2-molar equivalent (reagent:alkyne) of 4-azidobenzaldehyde (Santa Cruz Biotechnology, sc-503201) or Ald-CH_2-PEG_3-Azide (BroadPharm, BP-21715) was dissolved in DMSO (100 mg mL^{-1}). Sodium ascorbate and copper stock solutions were then added to a final concentration of 4.52 mM and 0.24 mM, respectively. Lastly, the Bza- or Ald- containing small molecule was added and the solution was then degassed and left to reaction for 24 hours at RT in the dark.

After 24 hours, an equal volume amount of 50 mM EDTA pH 7.0 was added to the reaction and stirred at RT for 1 hour. The solution was then further diluted ~5X with DI water and sterile filtered using a 0.22-μm filter to remove any copper precipitates. The resulting solution was dialyzed against 4-L of ultra-pure deionized water that was routinely changed every 12 hours over the course of 3 days. The final dialyzed product was then sterilized using a 0.22-μm syringe filter, frozen, and lyophilized for 3 days in a sterile, filtered 50 mL tube.

2.4 Oxidation of Hyaluronic Acid:

The oxidation reaction of HA has previously been reported elsewhere [39,40]. In short, 1.5 MDa HA (sodium salt) (Millipore, 53747) is first dissolved in DI water at 4 mg mL^{-1}, overnight, at 4 °C with constant agitation. The following day, sodium periodate is dissolved in DI water to a final concentration of 0.1 M, and added dropwise to the HA solution to a final volumetric ratio of 1:5. After addition of sodium periodate, the reaction vial is covered in aluminum foil and left to react for the desired amount of time at RT. In the present manuscript, HA was oxidized for either: 8 hours (HA8), 16 hours (HA16), or 24 hours (HA24). Following the desired oxidation time, ethylene glycol is added to inactivate any

unreacted periodate. After one hour of deactivation, the reaction volume is transferred to dialysis tubing and dialyzed against 4-L of ultra-pure deionized water. The 4-L of dialysis water is routinely refreshed every 12 hours over the course of 3 days. The final dialyzed product is then sterile filtered using a 0.22-μm syringe filter, frozen, and lyophilized for 3 days.

2.5 Hydrogel Formation:

For the HELP system, ELP is dissolved over night at a concentration of 4% (w/v) in sterile 1X PBS at 4 °C. In tandem, HA is dissolved over-night at 4% (w/v) in 10X PBS at 4 °C. The following day, equal-volume amounts of HA and pre-chilled 1X PBS are mixed on ice. The resulting 2% HA solution is then mixed with an equal-volume amount of 4% ELP on ice by careful pipetting to produce a final concentration of 2% ELP and 1% HA in 2.5X PBS. For the Matrigel hydrogels, appropriately sized aliquots of commercial Matrigel (Thermo, CB-40230) are thawed overnight. Then, the thawed Matrigel is supplemented with 1X PBS (final: 12.5% (v/v)) and mixed on ice by careful pipetting, ensuring no bubbles are introduced.

2.6 Hydrogel Stiffness and Stress-Relaxation Measurements:

Shear-rheology was carried out on a stress-controlled ARG2 rheometer (TA Instruments) using a 20-mm diameter, cone-on-plate geometry. All tests were conducted on 50-μL hydrogel samples, and heavy mineral oil was used to fill the gap between the rheometer geometry and external environment to ensure hydration over the course of all measurements. Representative values are composed of 3 – 5 replicates per gel formulation.

Samples were first crosslinked at RT, and a time sweep was measured over the duration at a strain of 1% and oscillatory frequency of 1 rad s^{-1}. Gelation was first indicated by the crossover point, where the storage modulus (G') was observed to be greater than the loss modulus (G''). After sufficient time (HELP Gels, 30 min; Matrigel, 1 hour) all gels reached a stable plateau modulus, and the sample temperature was ramped to 37 °C (3 °C min^{-1}). Gels were then incubated at 15 min at 37 °C to ensure complete cross-linking. The shear modulus for each sample was measured at 37 °C using a frequency sweep over the oscillatory frequency range of 0.1 – 10 rad s^{-1} at a fixed strain of 10%. Complete gelation at this stage was further confirmed by demonstration of a stable (linear) G' over the measured frequency range, and a final stiffness value for each gel was reported as the shear moduli at 1 rad s^{-1} and average. Following each frequency sweep, samples were incubated at 37 °C for 5 minutes at 1% strain and a frequency of 1 rad s^{-1}. Afterwards, the sample was strained to 10% and the stress was measured as a function of time over 12 hours. As an indicator of the stress-relaxation property for each gel, the time to reach half of the initial stress ($t_{0.5}$) has been reported.

2.7 Hydrogel Injectability Screening:

Prior to *in vivo* testing, we screened our HELP gels for relative ease of injectability. Three criteria were used to assess ease of injectability: (1) Injectability post complete gelation ($t_{crosslink}$ > 30 min), (2) injectability with one hand through a 30 G, hooked, needle and (3) degree of 'burst' injection. For testing, 50-μL samples of HA24, HA16, HA8, HA-A,

and HA-B hydrogels supplemented with food coloring (Market Pantry) were loaded into the back of a 30-G syringe (Fisher, 13–689-15). Following back loading, HELP gels were crosslinked at RT for 30 minutes. The needle tip was carefully hooked using a pair of surgical forceps to an angle of approximately 90° with a 2 mm tip to simulate injection conditions. Each hydrogel was then injected by hand, and a video was recorded for future assessment and reference. Immediately following injection, successful completion or failure of each criterion was rated, with a check mark (✓) being given for complete success and a x-mark (x) being given for a non-satisfactory result, respectively.

2.8 Fracture Stress Measurement:

Fracture stress measurements were carried out on a stress-controlled ARG2 rheometer (TA Instruments) using a 20-mm diameter, cone-on-plate geometry. All tests were conducted on 50-μL samples prepared in accordance with the above protocols. Heavy mineral oil was used to fill the gap between the rheometer geometry and external environment to ensure hydration over the course of all measurements. Samples were first crosslinked at RT, and a 30-minute time-sweep was measured at a strain of 1% and oscillatory frequency of 1 rad s^{-1}. Following 30 minutes of crosslinking, HELP gels were exposed to a repeated creep test wherein the % strain (γ) was measured over the course of a three-minute duration of an applied, fixed, stress (σ). After each stress step the material was allowed to relax ($\sigma = 0$) for 15 min to recover any accumulated strains. This cycle was repeated, with each subsequent stress being twice as high as the former (e.g., $\sigma = 1\ Pa$, 2 *Pa*, 4 *Pa*, 8 *Pa*), up until a stress that finally induced failure of the material (% strain > 2000%).

From these data, we generated plots of the viscosity as a function of the applied stress. Using Newton's law of viscosity, we calculated a strain rate ($d\gamma/dt = \dot{\gamma}$) and subsequently the apparent viscosity ($\eta = \sigma/\dot{\gamma}$) as a function of stress (Eq. 1). The stress state that induced an abrupt decline in viscosity ($\eta \rightarrow 0\ Pa\ s$) was taken to indicate the fracture stress (σ_F) of the material. Reported values are composed of 4 – 5 replicates per gel formulation and averaged.

$$\sigma = \eta \cdot \dot{\gamma} \rightarrow \eta = \frac{\sigma}{\dot{\gamma}} \quad \text{Eq. 1}$$

2.9 PEGylation of Fluorescent Microspheres:

To serve as a simulated cargo encapsulated fluorescent 10-μm diameter polystyrene latex microspheres (Polysciences, 18142–2) in our HELP gels. To facilitate a monodisperse mixture, the microspheres were PEGylated with 2,000 Da Poly(ethylene)glycol (PEG) diamine molecules (Sigma, 753084). This protocol has been reported previously [41]. First, the microsphere stock solution was vigorously vortexed for 60 seconds. After vortexing, 100 μL of stock suspension was transferred to a 1.5 mL tube, centrifuged, and pelleted. The storage buffer was carefully decanted, and then the pelleted microspheres were resuspended with 200 μL of 50 mM MES buffer, pH 6.0, and washed. Washing is repeated for a total of three cycles, and the microspheres are finally re-suspended in 200 μL MES buffer. Next: (1) 2 mM solution of bifunctional, amine-terminated PEG in 100 mM bicarbonate buffer, (2) 200 mM EDC (Thermo, 22980) suspended in 50 mM MES buffer, and (3) 500 mM

sulfo-NHS (Thermo, 24510) in 50 mM MES buffer were prepared. 2 μL NHS (final: 5 mM) and 2 μL EDC (final: 4 mM) were added sequentially and vortexed. The reaction proceeded for 30 minutes at RT. After reacting, 200 μL PEG-diamine (final: 50mM) was added and mixed by vortexing before incubating for 30 at RT. The reaction was quenches by the addition of 400 μL 200 mM glycine in PBS (final: 100 mM) and mixed by vortexing. A final 30 minute RT incubation step was then conducted. The microsphere solution was then centrifuged at 9,000 x g for 3 minutes and carefully decanted. Microspheres were re-suspended in 800 μL ultra-pure DI water and mixe by gentle pipetting. This process was repeated, each time lowering the suspension volume by 200 μL. After the 4^{th} wash (re-suspending in 200 μL ultra-pure DI water), two additional washes were performed. The microspheres were then centrifuged at 9,000 × g for 3 minutes, aspirated, and re-suspend in ultra-pure DI water to a final concentration of 2% (w/v).

2.10 Surgical Procedure, Animal Post-Op Care, and Euthanasia:

This protocol was approved by the Stanford Administrative Panel on Laboratory Animal Care. The National Institutes of Health (NIH) guidelines for the care and use of laboratory animals were observed (NIH publication no. 85–23 Rev. 1985). All animals were purchased from Charles River and caged in gender-matched pairs for the duration of this protocol. Food and water were administered ad libitum, and their environment was temperature and humidity controlled with a 12-hour on, 12-hour off light schedule. Animals were checked every day over the course of the experiment for any signs of distress or injury to ensure a safe environment. Animals that showed evidence of distress or injury were euthanized.

First, mixed-gender Sprague Dawley rats (10-week-old, n=38; 19♂ 19♀) were anesthetized using 3% isoflurane mixed with 1% oxygen for 10 minutes and then intubated using a silicone, 16-G catheter sheath (Santa Cruz Biotech, sc-360107). Rats were hooked up to a mechanical respirator (Harvard Apparatus, 55–7040) with 1 – 2% isoflurane and 1% oxygen to allow for mechanical ventilation (~2 – 3 mL push volume, 80 BPM). The chest was cleared of all fur and a left thoracotomy was performed to expose the heart. Once the wall of the left ventricle was identified, an injection of 50 μL of hydrogel was administered. All injections were carried out by hand, and the needle tip was left inside the heart wall for approximately ~10 seconds to minimize acute reflux. After stable cardiac rhythm had been recovered, the chest cavity was closed with 4–0 absorbable sutures (Thermo, NC1656516) and the negative pressure of the chest cavity was restored. The chest muscles and skin were closed using 4–0 absorbable sutures. Following skin closure, rats received subcutaneous injections of buprenorphine SR (1.5 mg kg^{-1}), bupivacaine (0.25%), and carprofen (0.5 mg mL^{-1}). The isoflurane gas was then cut off and the animal was mechanically ventilated with 1% oxygen until they woke. Animals were then placed into a warm recovery chamber with circulating 1% oxygen for an additional 15 – 30 minutes and monitored for signs of movement and recovery, after which the rat was returned to their housing which was warmed with a heating pad. For 3 days post-surgery, rats received a daily injection of carprofen (0.5 mg mL^{-1}) while under light passive inhalation anesthesia (1.5% isoflurane). If any animal was found in catatonia, immobile/paralyzed, and/or lost more than 10% of its pre-operative body weight, it was euthanized as per the Stanford Administrative Panel on Laboratory Animal Care.

Prior to euthanasia, rats underwent inhalation anesthesia using 3% isoflurane within a knock-down chamber and were then transferred to a standard nose cone. The lateral tail veins were visualized by placing the tails in a beaker of warm water to promote vasodilation. Once the veins were adequately visualized, rats were euthanized via intravenous injection of potassium chloride (90 mg mL^{-1}) using a 26-G needle.

2.11 Heart Dissection and Fixation:

Following euthanasia, the chest was shaved of all fur and cleaned using 70% ethanol. The skin, underlying muscle, and bones of the rib cage were removed, and the exposed heart was excised using surgical scissors. The outside of the heart was washed with fresh, sterile, 1X PBS, and then manually perfused with gentle prodding. After perfusion, a 5-mm section of the heart, roughly centered around the injection site, was removed using a pair of fresh razor blades and a heart matrix sectioning tool (Zivic Instruments, HSRS001–1). The 5-mm section of heart was immersed in 40 mL of ice-cold, freshly prepared 4% paraformaldehyde and fixed for 72 hours at 4 °C. After fixation, the tissue section was transferred to fresh, 30% sucrose in PBS for 72 hours.

2.12 Tissue Embedding, Gelatin-Coating Slides, and Tissue Sectioning:

All tissue sections were embedded in optimal cutting temperature (O.C.T.; Thermo, 23–730-571) by snap freezing. A metal bowl was filled with 100% ethanol and rapidly cooled by chilling with dry ice. Tissue sections were removed from 30% sucrose solution, gently dried, and immersed in O.C.T. media in a disposable embedding mold (Fisher, 1380). Molds were then carefully placed into chilled, 100% ethanol. Once the sample block was frozen samples were then stored in a −80 °C freezer until sectioning (minimum of 24 hours)

All tissue samples presented herein were sectioned on a cryostat (Leica). Prior to sectioning, tissue samples were transferred to −20 °C for 48 hours. Sections were then mounted on a metal puck with excess O.C.T. and sectioned into 20-μm thick slices. Because of the relatively large volume of the injection site, tissue samples were collected at semi-regular intervals with a target spacing of 120 μm between cuts and a total of ~45 tissue sections collected from each heart.

2.13 Tissue Imaging:

To ensure an approximately equal number of sections were imaged for microsphere and hydrogel retention, 8 slides with 2 – 3 semi-regularly sectioned tissue slices were selected from 15 total slides collected per animal. After warming slides to RT, they were then incubated at 37 °C for 30 minutes and subsequently rinsed in tap water for 5 minutes. ProLong Gold anti-fade media (Cell Signaling, 9071S) and a coverslip (Thermo, 3323) were used for mounting and sealing. Slides were left to cure at RT in a shadow box for 72 hours.

Fluorescent imaging was performed on a Leica Thunder Inverted microscope. Images were taken as tile scans that varied in physical dimensions based on the area of injectate, but on average had dept physical height of ~60 μm (3.80-μm step size). Tile-scans were stitched together within the Leica software (LASX) and additionally clarified using the Leica Thunder & Lightening computational clearing algorithm to remove background noise.

All images are presented as max projections, compiled, and exported in ImageJ (ImageJ opensource software) [42].

2.14 Microsphere Retention Quantification:

Quantification was carried out in three steps: (1) image analysis in Fiji (ImageJ opensource software) [42] (2) post-processing data with an automated Python script and (3) final tabulations in Excel (Windows). First, the microsphere channel was isolated. Using ImageJ macro scripting all images to binary images and quantified for microsphere content using a particle counter script in Fiji (ImageJ opensource software) [42,43]. To account for microsphere clustering, we used a secondary Python script that divided the calculated area (px^2) of every particle in an image by the average cross-sectional area of a microsphere (~ 71 px^2). Based on these values, we were able to estimate the number of microspheres that were undercounted in each image from clustering and then added these values to the respective image count to obtain a more accurate estimate.

To tabulate the number of microspheres within the injection site, we summed two values over the total number of images (N): (1) the total microsphere count from each individual image (B_i) and (2) an estimation of the microsphere count between two image slices ($B_{int,\,j}$; Eq. 2). To estimate the number of microspheres between two sequential tissue slices, we assumed that there was a linear transition in the microsphere count between them. By recording the number of tissue slices (n) that were discarded between two adjacent sections we estimated the number of microspheres in each slice and summed them (B_{int}). The general form of this equation has been provided (Eq. 3).

$$Beads = \sum_{i=1}^{N} B_i + \sum_{j=1}^{N-1} B_{int,\,j} \qquad \text{Eq. 2}$$

$$B_{int,\,j} = \sum_{j=1}^{n} \left[B_i + j(B_{i+1} - B_i)\left(\frac{1}{n+1}\right) \right]$$

$$B_{int,\,j} = \frac{n}{2}(B_i + B_{i+1}) \qquad \text{Eq. 3}$$

2.15 Hematoxylin and Eosin Staining:

From each animal, a single representative slide with 2 – 3, 20-μm, thick heart sections were removed from −80 °C storage. The slide was warmed to RT, incubated at 37 °C for 30 minutes and subsequently rinsed in tap water for 5 minutes. After washing, all slides were carried through the following general protocol. Hematoxylin stain for 3 minutes; rinse with tap water for 1 minute; immerse in clarifying solution for 1 minute; rinse in 95% ethanol for 1 minute; stain with eosin for 30 seconds. Slides were then dehydrated through a step-down process. Briefly, 95% ethanol for 1 minute; two successive washes with 100% ethanol for 1 minute each; 2 successive washes with Xylene for 2 minutes each. After dehydration, slides

were left to dry then covered with mounting media and a coverslip. All slides were imaged and digitized on an Aperio AT2 (Leica) slide scanner using a 50X air objective and stitched together and viewed in Image Scope (Leica).

2.16 Data Analysis and Statistics:

All data are presented as mean ± standard deviation (SD), with individual replicate values indicated by a black circle (•). Replicate count is either listed in the figure directly or in a corresponding methods section. Statistical significance testing for all data was performed in the GraphPad Prism 9 software package. The specific test for each data has been listed in the corresponding figure cation. Presently we use a significance cutoff of $\alpha = 0.05$ and a relevant post-hoc test. In all figures, significance cutoffs are defined as follows: * $p < 0.05$; ** $p < 0.01$, *** $p < 0.001$, **** $p < 0.0001$, or ns for not significant.

3. Results and Discussion.

3.1 HELP variant synthesis and mechanical characterization:

Our work was motivated by the clinical need for materials with mechanical properties that both allow catheter injectability and significant retention within the contracting myocardium. Due to their low viscosity, saline or medium are commonly used as a catheter-injectable delivery systems, yet their ability to retain therapeutics within the myocardium is low [44–49]. Previously, our two-component hyaluronan (HA) and elastin-like protein (ELP) hydrogel (HELP) system was used to deliver cells and miRNA to the heart [50], yet no quantitative measurements of retention were performed. This leaves it unclear as to which material properties were most relevant for allowing injectability and affecting down-stream retention. To address these questions, we synthesized a family of five HELP hydrogel variants with distinct material properties to determine their effects on injectability.

Our HELP gel system is a dynamic covalently crosslinked (DCC) polymer network. Upon mixing, the hydrazine-functionalized elastin-like protein (ELP) forms a DCC hydrazone linkage with aldehyde-functionalized hyaluronan (HA). The recombinant ELP (full amino acid sequence in Figure S1) was expressed in *Escherichia coli*, purified through temperature cycling, and conjugated with hydrazine moieties [38] (12.28 hydrazine groups per ELP; representative NMR in Figure S2). To modulate the final gel mechanics, we synthesized 5 distinct HA variants that would allow us to systematically study the effects of gel material properties on injectability and down-stream retention.

We employed two HA modification schemes to add aldehyde moieties: 1) sodium periodate oxidation and 2) bio-conjugation. Oxidizing HA with sodium periodate results in opening of the HA carbon rings and formation of a di-aldehyde group at the oxidation site [51]. In addition, extensive oxidation leads to backbone cleavage and chain length shortening [51,52]. Importantly, these changes are expected to vary with oxidation time. To provide a range of HA properties we tested three oxidation times: 8, 16, and 24 hours yielding HA8, HA16, and HA24, respectively. As an alternative to oxidation, we employed bio-conjugation, which positions the aldehyde moieties as pendant side-groups and conserves the structure of the HA rings. We made use of two commercially available small molecules

to append either aldehyde (HA-A) or benzaldehyde (HA-B) side-groups, which are known to have fast and slow exchange kinetics, respectively [53]. Together, these 5 polymers were expected to present a spectrum of material properties, allowing us to study the underlying materials science design rules that improve hydrogel injectability and myocardial retention. A schematic representation of these modification routes are summarized in Figure S3.

The degree of functionalization for our oxidized groups was quantified using a modified TNBS assay [40]. Our results, interestingly, show a decrease in observed oxidation with oxidation time, with measured oxidation levels of 29.2%, 14.1%, and 10.4% for HA8, HA16, and HA24, respectively (Figure S4). To our knowledge this trend has not been reported elsewhere. However, others have reported a diminishing return in terms of predicted oxidation versus that observed, with higher molar ratios of periodate to HA yielding progressively lower efficiencies of oxidation [54]. This plateauing effect as observed by others may suggest a theoretical maximum degree of oxidation for a given molar ratio (here we use 1:1 periodate:HA monomer), after which the number of available aldehydes may begin to decline due to side reactions with hydroxides on unoxidized hydroxyl residues forming HA rings [51]. We additionally quantified the degree of functionalization of our bio-conjugated HA through NMR, and measured an approximate 12% degree of modification (Figure S5). An important consideration is that oxidation results in formation of two aldehyde groups, so the number of aldehyde groups available for crosslinking in HA24 and HA16 is almost twice as high as our bio-conjugated groups, and HA8 has nearly 4 times more aldehydes, which is expected to impact the resulting stiffness.

The oxidation of HA is also known to significantly reduce the molecular weight [55], compared to bio-conjugation which is not expected to alter the overall HA M_w. Using gel permeation chromatography (GPC), we characterized the molecular weight of our experimental HA groups as well as an array of commercially available, unmodified, HA samples (M_W range of 20 kDa to 1.5 MDa) as controls (Figure S6A – C). Consistent with the work of others, we found that the molecular weight of our oxidized variants significantly decreased with oxidation time, with the initial M_W of 1.5 MDa dropping to an apparent M_w of 177 kDa, 80.1 kDa, and 56.8 kDa for HA8, HA16, and HA24, respectively. Interestingly, the HA variants synthesized by bio-conjugation chemistry appeared to have an increase in M_w shifting from an initial M_W of 100 kDa to an apparent M_W of 221 kDa and 141 kDa for HA-A and HA-B, respectively. These observed molecular weights are somewhat larger than the theoretically predicted M_W for a 12% HA modification reaction, which are 115 kDa and 105 kDa for HA-A and HA-B when accounting for additional mass from side groups. This discrepancy is likely due to the bulky and hydrophilic side-chains causing the HA polymer chain to expand and produce an artificially high M_w in GPC, which is size-based. We further confirmed this by using dynamic light scattering (DLS) wherein we measured the hydrodynamic radius (R_h) of our different groups (Figure S6D – F). Consistent with our M_w trends in GPC, unmodified, 100 kDa HA and 12% modified HA-Alkyne had a measured R_h of 10.56 nm and 10.95 nm, respectively, while HA-A and HA-B had R_h of 14.48 nm and 11.51 nm, respectively. Collectively, these data suggest that there was a greater change in the HA M_w following the addition of the final side groups, which in turn likely contributed to an over-prediction of the observed M_w by GPC.

To probe how these different modification schemes influenced gel mechanics, we kept the overall gel concentration the same: 2% (w/v) ELP and 1% (w/v) HA but varied the HA type. Using oscillatory shear rheology, we found that all five formulations showed evidence of gelation (storage modulus (G') > loss modulus (G")) in under 30 seconds (Figure S7); Additionally, after 30 minutes of crosslinking at room temperature (RT), all five gels had reached a stable plateau modulus suggesting complete gelation (Figure S6). Following a final heating step to 37 °C we tabulated a maximum shear modulus (Figure 2A) and stress-relaxation rate (Figure 2B) from 3 – 5 independent replicates and found that both properties can be significantly changed by altering the identity of the HA component. Tabulated averages are presented in Figure 2C, and representative frequency sweeps (Figure 2D), and normalized stress-relaxation curves (Figure 2E) are provided for reference.

These data indicate that by changing the degree of modification, M_w, and crosslinking kinetics of the HA component, we can significantly modulate the resulting shear modulus between ~490 Pa and ~3200 Pa. For our oxidized HA variants, increased oxidation time resulted in more compliant gels, which is attributed to 1) fewer available aldehyde crosslinking sites (Figure S4) and 2) shorter HA M_w (Figure S6). It is interesting to compare the HA-A and HA24 formulations, which have similar shear moduli (~500 Pa). The HA-A formulation has an aldehyde:hydrazine ratio ~1:2 and HA M_w of ~100 kDa. In comparison, the HA24 formulation has an aldehyde:hydrazine ratio ~1:1 and HA M_w of ~40 kDa. Taken together, this suggests that despite the potential for more complete crosslinking in HA24 due to the ideal stoichiometric ratio, the decreased M_w may lead to defects in the network structure, such as looping of a single HA chain back to the same ELP polymer, which decreases overall stiffness. Another interesting comparison is the HA-A and HA-B formulations. Despite having similar stoichiometric ratios of crosslinking functional groups, HA-A had a significantly lower shear modulus than HA-B. Consistent with reports from others comparing aldehydes and benzaldehydes [53], HA-A had much faster reaction kinetics than HA-B (gelation time < 30 sec for HA-A and 3 minutes for HA-B, Figure S7). Thus, HA-B is likely to form a more homogenous network, which would lead to more effective crosslinking and a stiffer gel.

Similar to matrix stiffness, we see that HA material properties significantly influence the final gel stress-relaxation time, with $t_{0.5}$ ranging between ~0.51 hr to ~13.6 hr. As excepted, the biggest determining factor in stress-relaxation rate is bond kinetics, with the HA-B formulation exhibiting the longest $t_{0.5}$ owing to its relatively slow exchange kinetics. Within the faster kinetics, aldehyde-bearing formulations (HA24, HA16, HA8, and HA-A) the trend in observed stress-relaxation time is similar to matrix stiffness: HA24 and HA-A are statistically similar, and HA16 and HA8 have progressively longer stress-relaxation times.

As a point of comparison, Matrigel, a common injectable hydrogel, has a measured shear stiffness that is an order of magnitude lower than our softest HELP gel variant; ~39 Pa). Similarly, when using the same testing protocol to characterize stress-relaxation we found that it was much faster having a $t_{0.5}$ (at 10% strain) of ~67 (Figure S8). It is commonly hypothesized that hydrogels with more robust (i.e., stiffer) mechanical properties may increase retention due to its ability to resist mechanical expulsion from the beating myocardium. Similarly, the rate of erosion of hydrogels using reversible linkages (such

as those in HELP gels) have been linked to stress-relaxation in the literature [56], with faster exchange kinetics leading to a more rapid erosion which may have implications for long-term retention. Taken together, injectable gels that have both a higher stiffness and slower stress-relaxation may be able to increase both acute and long-term retention. As highlighted here, both of these properties are subject to significant changes based on the modification scheme which further shows the importance in a meticulous understanding of structure-processing relations in altering the final hydrogel mechanics to maximize retention.

3.2 Qualitative evaluation of in vitro injectability:

Following mechanical characterization, we further screened our HELP gel variants for ease of injectability. DCC polymer networks based on hydrazone linkages have been shown by our group to be shear thinning and injectable [35]. However, 'ease' of injectability is nebulous. To better rate the qualitative injectability of our materials, we identified three criteria vital to facilitating repeatable injections (Figure 3A). First, (1) we assessed which gels were injectable through a 30-G needle following complete crosslinking (30 minutes). While many injectable gel formulations are designed to crosslink *in situ*, this often results in a narrow time window within which the gel can be injected. If injection is carried out prior to gelation, the material can flow away from the target injection site or be ejected out of the contracting myocardium. In contrast, if the surgeon injects too late or too slowly, then premature crosslinking can result in a clogged needle and failed delivery. Designing a gel that can be injected post-crosslinking overcomes these limitations. (2) Of those formulations that are injectable post-gelation, we assessed which gel formulations could be injected with only one hand by an experienced surgeon. (3) Finally, as a third criterion, we characterized of the gels that could be injected, which of them had evidence of a 'burst' injection. While excessive force can be used to pass a material through a needle deeming it 'injectable', materials that require a higher amount of force may inadvertently cause trauma to the local tissue environment due to the ejection pressure.

As an additional consideration, it is known that our unmodified ELP undergo a lower critical solution temperature (LCST) phase transition into protein-rich and protein-lean regions at approximately ~32 °C – 33 °C [57]. This temperature shift, theoretically, could impact the relative ease of injectability depending on the temperature at which injections are performed. From a translational perspective, most injections are expected to occur at room temperature making it a potentially more relevant injection condition to test. However, to give better context to our injection testing in light of the mechanics measured previously we opted to measure the LCST of our ELP pre- and post-modification as the LCST range is related to the overall hydrophobicity of the protein which is modified by functionalization. Our optical density measurements indicate that following functionalization, the LCST of ELP increased to approximately 38 °C - 39 °C (Figure S9A), suggesting that thermal aggregation would be expected to minimally impact the final mechanical property of our hydrogels. We further verified this by comparing the shear moduli pre- and post-thermal incubation at 37 °C (Figure S9B). Taken together, we posit that the mechanical properties measured previously (at 37 °C) are expected to be similar to those injected presently at room temperature.

To mimic the protocol for preclinical injection studies, 50 μL of HELP gel at a final concentration of 2% (w/v) ELP and 1% (w/v) HA was made for each HA-variant and injections were repeated in triplicate (Figure S10, Figure 3B, 3C). From our test groups, we found that only two of our five HA-variants, HA24 and HA16, met all three criteria. The HA-8 and HA-A variants could be injected post-crosslinking, but required the surgeon to use both hands to apply an adequate amount of force. In our experience, stabilization of the injecting hand is required to limit tissue damage and ensure smooth injection, and so gels that require the use of both hands pose increased risk to the animal and a higher degree of variability. We additionally found that both HA8 and HA-A had evidence of a 'burst' injection where all (HA8) or a large fraction (HA-A) of the material appeared to shoot out of the needle during. Further, we found that HA-B could not be injected.

Based on the encouraging results of our injectability study with a 30-G needle we aimed to validate clinical feasibility using a catheter delivery system. As a proof-of-concept demonstration, we injected 700 μL of HA16 through a 150-cm medical catheter (Figure S11). While a greater amount of hand force was needed to move the material through the entire length of the catheter compared to the shorter, 30-G needles, the gel was smoothly ejected with a steady flow from the tip of the catheter (*i.e.,* no "burst" injection). This suggested that HELP gels could potentially be implanted via intravenous delivery which is vital to side-stepping the need for thoracic-level surgeries for implantation.

3.3 Quantitative assessment of gel failure stress and yield stress:

Following *our in vitro* injectability study, we sought to characterize which mechanical properties of our five hydrogel systems best served as a 'predictor' for injectability. Based on our initial mechanical characterization, there did not appear to be a direct relationship between either the initial matrix stiffness nor the stress-relaxation time (as indicated by $t_{0.5}$) (Figure 2C,E) and ease of injection. HA-A, for example, was both 'softer' (more compliant) and had a shorter stress-relaxation time than HA16, but was markedly harder to inject through a 30-G needle. Given that the injection occurs post complete cross-linking, and on a time scale that is much faster than the stress-relaxation time of our hydrogels, we hypothesized that injectability is not tied to the reversibility of the hydrazone linkages and thus may be plastically deforming the hydrogel through a mix of bond and chain breaking, as has been suggested previously [55,58,59].

To test this hypothesis, we ran a two-part recovery experiment looking at mechanics immediately following injection of HA24 and HA16 using a low stain (1%) time sweep, and then assessed hydrogel bulk mechanics using a high strain (10%) frequency sweep following 24 hours of recovery. Our measurements show that post-injection the gels rapidly begin to self-heal after injection, as evidenced by $G' > G''$ (Figure S12A, B). After 24 hours of incubation post-injection, both gels reached an approximate plateau shear modulus of ~300 Pa. Notably, this plateau shear modulus is lower than the pre-injection plateau modulus; ~450 Pa and ~730 Pa for HA24 and HA16, respectively (Figure S7), suggesting that full network recovery is not achieved. Consistent with these data, our post-recovery high strain test (10%) shows that both HA16 and HA24 cannot sustain high strain deformation and enter the sol phase ($G'' > G'$, Figure S13A, B, respectively) under this condition.

Taken together these data support the conclusion that injection of HELP gels plastically deform the network leading to a state of flow, potentially breaking the into discrete gel "blobs" that flow with "plug-flow" fluid dynamics [60]. Following ejection, the observed recovery in bulk gel mechanics is potentially facilitated through hydrazone bond formation due to dense microgel packing (sometimes termed a "granular hydrogel" [61,62]). Other dynamic hydrogels, including those formed through peptide and protein self-assembly mechanisms, have been reported to have similar flow mechanisms [55,58,59].

To probe this theory of gel failure stress being tied to injectability, we ran a series of successive creep tests at progressively higher stress (σ) states and measured the responsive strain (γ) of our hydrogels (representative tests reproduced in Figure S14) to investigate for yielding behavior, which would suggest the onset of plastic deformation. From these data, we calculated a strain rate ($d\gamma/dt = \dot{\gamma}$) for each stress state, and by applying Newton's law of viscosity (Eq. 1), we determined the apparent viscosity (η). Given that the apparent viscosity is linear within the elastic regime ($\eta = \sigma/\dot{\gamma}$), we aimed to estimate the apparent yield stress (σ_y) and fracture stress (σ_F) by monitoring for deviation from linearity in η. In the present work, we define η σ_y as the stress-step that induces a permanent deformation (% $\gamma \gg 0$ after the relaxation period) and σ_F as the stress-step that induces failure of the gel ($\eta \rightarrow 0$).

For all five HELP gels, prior to yielding, the apparent viscosity calculated across successive stress steps was linear (Figure 4A), suggesting that our testing parameters were appropriate. For HELP gels produced through oxidation chemistry (HA24, HA16, HA8), we did not observe evidence of yielding behavior across this range of applied stresses whereas HELP gels produced through bio-conjugation reactions (HA-A and HA-B) showed signs of yielding as evidenced by an irrecoverable strain above a certain applied load (Figure S14). Multiple, independent replicates (n = 4 – 5) of each HELP gel variant were tested to characterize the average fractures stress (Figure 4B), which was tabulated for all gels (Figure 4C). The observed fracture stress ranged from approximately ~170 Pa to ~12,000 Pa, following HA24 < HA16 < HA8 < HA-A < HA-B. Importantly, we point out that these data parallel our qualitative *in vitro* screening of injectability (Figure 3). Taken together, our data suggest that σ_F may be a critical indictor of HELP gel injectability, which is consistent with similar findings in the literature [55].

It is interesting to consider, how the different HA polymeric properties (Figures S4, S5, and S6) may be influencing injectability. First, there does not appear to be a direct relationship between the observed stress-relaxation time and injectability, as both our fastest (HA-A) and slowest (HA-B) stress-relaxing gels had the two highest reported σ_F values and were not injectable with only one hand. Within our oxidized gels (HA8, HA16, and HA24), we observe that gels using HA with longer oxidation times have lower fracture stress and easier injectability (Figures S14, Figures 3, 4). This is likely due to a combination of both (1) a reduction in chain entanglements due to lower M_w and (2) fewer aldehyde functional groups available for crosslinking. An additional interesting observation is the difference in mechanism of failure: our oxidized systems (HA8, HA16, and HA8) appear brittle with a lower failure stress, while our bio-conjugated formulations (HA-A and HA-B) display some yielding behavior before failure and a higher failure stress. One possible explanation for this is the difference in the HA backbone structure; the oxidized chains likely have greater chain

flexibility and a higher propensity for cleavage due to the opening of their HA carbon ring structure during oxidation.

3.4 In vivo preclinical retention study

To test the *in vivo* efficacy of our injectable HELP variants (HA24 and HA16), we quantified the relative retention of 10-μm fluorescent microspheres injected directly into healthy, beating rat myocardium both 1 day and 7 days post-injection. As a control we have also chosen to include Matrigel which is a frequently used delivery vehicle [30,63,64]. The choice of using a healthy, rather than a diseased or injured, murine model was made (1) to increase reproducibility (injury models like typically result in a range of infarct lesion sizes [65]), and (2) to test injection and retention of cargo in the most challenging *in vivo* system, the strongly contractile healthy myocardium [26,27], allowing us to expose our materials to a reproducible, challenging mechanical environment.

For cargo quantification, all gel samples (HA16, HA24, and Matrigel) were loaded with the same concentration of fluorescent beads, 1.25 mg mL^{-1}, to allow cross-comparisons. Additionally, for HELP gels (HA16 and HA24), 20% (v/v) of the ELP peptides were labeled with a fluorescent cyanine-5 group to allow for easier visualization of the gel. These concentrations and degree of labeling were determined through *ex vivo* screening to identify values that would enable automated image quantification (Figure S15). For our animal groups, 10-week-old Sprague Dawley rats were randomly divided into three, sex-matched tests groups: 1) HA16, 2) HA24, and 3) Matrigel, each with two cohorts for eventual end-point evaluation on either 1 day (Cohort 1) or 7 days (Cohort 2) post-injection (Table 1). A summary of mechanical properties (shear modulus and stress-relaxation) for our three test groups pre-injection have been reproduced for reference in Figure S16 for ease of comparison.”

Following a left thoracotomy, 50 μL of hydrogel with 1.25 mg mL^{-1} microspheres were injected by hand into the wall of the beating myocardium through a 30-G, manually hooked, needle (Figure S17). As a first point of measurement, we devised a four-part scoring system to rate the quality of our injections. The four criteria were: 1) degree of material ‘reflux’ out of the heart at the time of injection, 2) perceived ease of hand-injection into the heart by the surgeon, 3) degree of bleeding immediately following injection, and 4) accuracy of injection location within the wall of the left ventricle as determined by relative position to the left descending coronary artery. Across all three hydrogels, we did not observe a significant difference in the quality of injection for either cohort 1 or 2 (Figure S18). We observed similar degrees of bleeding post-injection across all three systems, suggesting that the observable trauma to local tissue may be invariant to the identity of the gel and that variability in bleeding is likely more closely tied to inherent variation in the local vasculature of the animals themselves. This further emphasizes the need for gels which can hold cargo at the injection site, as it has been proposed that one of the primary modes of cargo loss may come from rupturing the local heart vasculature and which results in injectate being evacuated from the injection site out of ruptured vessels [30,66,67]

Post euthanasia, hearts were excised, sectioned, and prepared (Figure S19). Microspheres were tabulated using a particle counter script in Fiji [42,43] (Figure S20), and quality

checked using a secondary Python script to account for microsphere clustering (Figure S21). Following image quantification, the approximate bead count was determined using Eq. 2 – 3 by summing the beads measured in each tissue section and interpolating the bead count between them (Figure 5A – F).

Qualitatively, we observed that HA16 and HA24 had a greater degree of spreading than Matrigel at both 1-day and 7-days post-injection. This was evidenced by (1) the relatively higher density of beads in Matrigel as compared to HA16 and HA24 as well as (2) the relative size of the injection cross section.

Based on our quantification, HA16 significantly improved the retention of fluorescent microspheres both 1- and 7-days post injection compared to Matrigel (Figure 6A). Based on our microparticle concentration, our intended cargo dosage is approximately ~70,110 microspheres per injection (Figure S15B). One-day post-injection, Matrigel retained approximately 16.9% ± 12.6% of the delivered microspheres compared to 53.6% ± 24.6% and 43.1% ± 30.3% retention for HA16 and HA24, respectively (Figure 6B, C). Interestingly, though non-intuitively, the target bead count increased at our 7-day time point for all three hydrogels; however, these differences were not found to be statistically significant (two-way ANOVA, post-hoc Tukey test) and are likely due to experimental error. We additionally note that when subdividing the animal cohorts by sex, we observed no differences in cargo retention (Figure S22).

As a final qualitative characterization, we stained representative sections with Hematoxylin and Eosin (H&E) (Figure 7). For all three hydrogels, we observed a clear increase in cell infiltration between 1- and 7-days post-injection, indicated by the increased number of nuclei (purple) within the bulk of the hydrogel. This cell infiltration may be assisted by the presence of the RGD cell-adhesive ligand present in the bio-active domain of the ELP. Future studies may explore using a previously reported, non-cell adhesive ELP variant, that includes a scrambled, RDG-sequence [38], to evaluate potential impacts on cell infiltration. We did not observe evidence of any uniform, fibrotic region surrounding the injected gels. These data encourage future detailed studies of gel biodegradation and the local immune response over time.

4. Conclusion

The hyaluronan and elastin-like protein (HELP) gel system presented here has several benefits compared to other currently available, injectable hydrogel systems. These include: (1) independent tuning of biochemical and biomechanical cues [36], (2) high degree of cell-compatibility [35–37], and (3) cell membrane protection during injection [35]. Additionally, hyaluronan (HA) has been shown to promote angiogenesis, suppress fibrous tissue formation, and natively bind water to the heart muscle, which improves mechanical and electrophysiological properties of the heart muscle [68–70]. While this injectable system has been shown to facilitate injection of cells and mRNA into the contracting myocardium [50], no quantification of retention was conducted, nor has there been any study of how processing affects injectability and retention leaving pathways for optimization unclear.

In the present manuscript, we screened a series of formulations of our two-component HELP hydrogel system for their mechanical properties (e.g., stress relaxation and matrix stiffness), *in vitro* injectability (qualitative injectability and failure stress), and finally the *in vivo* retention of microspheres following injection into the rat myocardium. Specifically, we modulated hydrogel mechanics by altering the HA modification scheme using both 1) sodium periodate oxidation and 2) bio-conjugation methods. Within our oxidized group, we generated three HAs by oxidizing HA for 8 ours (HA8), 16 hours (HA16), and 24 hours (HA24). Within our bio-conjugation group, we used a two-part chemical modification scheme where we ultimately attached fast (aldehyde; HA-A) or slow (benzaldehyde; HA-B) exchange rate groups to HA. Our mechanical testing indicated that both the shear modulus and stress-relaxation could be significantly altered by the modification scheme. Importantly, we show that the final structure of the HA following modification is critical in altering either of these properties Through a series of test-injections, we found that two formulations (HA16 and HA24) could be injected easily by hand through a 30-G needle, whereas the other systems either required excessive force resulting in a ‘burst’ injection (HA8, HA-A) or could not be injected at all (HA-B). Thus, lower polymer molecular weight and greater breakdown of the HA carbon ring structure are implicated in altering the ease of injection. In further probing the mechanics of injection, we found that injectability of our hydrogels correlated with failure stress (σ_F) as determined by shear rheology, suggesting that injection necessarily results in plastic deformation of our HELP gels. Finally, we conducted an *in vivo* retention study where we looked at the retention of 10-μm microspheres when delivered with (1) HA16, (2) HA24, or (3) commercial Matrigel directly into the healthy, contracting rat myocardium. Our results show that HA16 significantly improved cargo retention over Matrigel at both 1- and 7-days post injection, suggesting that HELP gels both inhibit acute reflux from the myocardium and may assist in long-term retention.

Looking ahead at translation of these gels to a preclinical injury model, some practical considerations may present limitations. First, the rate of gelation of our HELP gels is rapid (< 30 s), which makes homogenous mixing a challenge, especially for larger gel volumes, which would be required for any clinical-scale trials. A potential strategy to overcome this limitation could include use of static mixers to permit rapid, homogenous mixing. Another point of consideration is that when working with DCC networks, the stress-relaxation effect can be used to modulate cellular response, but it could also significantly influence the stability of the gels *in vivo*. On one hand, stress-relaxation has been shown to significantly influence cell-behavior and is a valuable control point when trying to modulate cell behavior for a given application [71]. However, from the standpoint of retention post-injection, DCC polymer networks, as with all dynamic networks, are susceptible to erosion and potentially more rapid biodegradation. Thus, future translation of DCC-based networks will need to carefully evaluate the *in vivo* erosion and biodegradation rate for optimization with the intended timeline of the therapy.

In summary, the HELP gel system was found to be easily hand-injectable through both syringe needles and catheters and to significantly improve the acute retention of cargo in the contractile myocardium. These data strongly support the future investigation of these materials for delivery of therapeutic agents to challenging environments such as mechanically active tissues.

Supplementary Material

Refer to Web version on PubMed Central for supplementary material.

Acknowledgements

We acknowledge N. Tran (Stanford; CA, USA) for assistance in performing the preclinical model. We thank T. Yamaoka, Y. Kanbe, and T. Takizawa (National Cerebral and Cardiovascular Center; Osaka, Japan) for preclinical model training. We acknowledge B. LeSavage (Stanford; CA, USA) for helpful conversations about statistical analyses and data presentation. We thank P. Chu and D. Wu (Stanford Human and Animal Histology Services, Stanford; CA, USA) for help with preparation of histological specimens. This work was supported by the National Institutes of Health (NIH) Training Grant in Biotechnology (T32-GM008412) to R.A.S. and R01 EB027666, R21 HL138042, and R01 HL151997 to S.C.H.

7. Data Availability

The raw data required to reproduce these findings will be made available upon request.

8. References

[1]. Lozano R, Naghavi M, Foreman K, Lim S, Shibuya K, Aboyans V, Abraham J, Adair T, Aggarwal R, Ahn SY, AlMazroa MA, Alvarado M, Anderson HR, Anderson LM, Andrews KG, Atkinson C, Baddour LM, Barker-Collo S, Bartels DH, Bell ML, Benjamin EJ, Bennett D, Bhalla K, Bikbov B, Abdulhak AB, Birbeck G, Blyth F, Bolliger I, Boufous S, Bucello C, Burch M, Burney P, Carapetis J, Chen H, Chou D, Chugh SS, Coffeng LE, Colan SD, Colquhoun S, Colson KE, Condon J, Connor MD, Cooper LT, Corriere M, Cortinovis M, de Vaccaro KC, Couser W, Cowie BC, Criqui MH, Cross M, Dabhadkar KC, Dahodwala N, De Leo D, Degenhardt L, Delossantos A, Denenberg J, Des Jarlais DC, Dharmaratne SD, Dorsey ER, Driscoll T, Duber H, Ebel B, Erwin PJ, Espindola P, Ezzati M, Feigin V, Flaxman AD, Forouzanfar MH, Fowkes FGR, Franklin R, Fransen M, Freeman MK, Gabriel SE, Gakidou E, Gaspari F, Gillum RF, Gonzalez-Medina D, Halasa YA, Haring D, Harrison JE, Havmoeller R, Hay RJ, Hoen B, Hotez PJ, Hoy D, Jacobsen KH, James SL, Jasrasaria R, Jayaraman S, Johns N, Karthikeyan G, Kassebaum N, Keren A, Khoo J-P, Knowlton LM, Kobusingye O, Koranteng A, Krishnamurthi R, Lipnick M, Lipshultz SE, Ohno SL, Mabweijano J, MacIntyre MF, Mallinger L, March L, Marks GB, Marks R, Matsumori A, Matzopoulos R, Mayosi BM, McAnulty JH, McDermott MM, McGrath J, Memish ZA, Mensah GA, Merriman TR, Michaud C, Miller M, Miller TR, Mock C, Mocumbi AO, Mokdad AA, Moran A, Mulholland K, Nair MN, Naldi L, Narayan KMV, Nasseri K, Norman P, O'Donnell M, Omer SB, Ortblad K, Osborne R, Ozgediz D, Pahari B, Pandian JD, Rivero AP, Padilla RP, Perez-Ruiz F, Perico N, Phillips D, Pierce K, Pope CA, Porrini E, Pourmalek F, Raju M, Ranganathan D, Rehm JT, Rein DB, Remuzzi G, Rivara FP, Roberts T, De León FR, Rosenfeld LC, Rushton L, Sacco RL, Salomon JA, Sampson U, Sanman E, Schwebel DC, Segui-Gomez M, Shepard DS, Singh D, Singleton J, Sliwa K, Smith E, Steer A, Taylor JA, Thomas B, Tleyjeh IM, Towbin JA, Truelsen T, Undurraga EA, Venketasubramanian N, Vijayakumar L, Vos T, Wagner GR, Wang M, Wang W, Watt K, Weinstock MA, Weintraub R, Wilkinson JD, Woolf AD, Wulf S, Yeh P-H, Yip P, Zabetian A, Zheng Z-J, Lopez AD, Murray CJ, Global and regional mortality from 235 causes of death for 20 age groups in 1990 and 2010: a systematic analysis for the Global Burden of Disease Study 2010, The Lancet. 380 (2012) 2095–2128. 10.1016/S0140-6736(12)61728-0.

[2]. Smolina K, Wright FL, Rayner M, Goldacre MJ, Determinants of the decline in mortality from acute myocardial infarction in England between 2002 and 2010: linked national database study, BMJ. 344 (2012) d8059. 10.1136/bmj.d8059. [PubMed: 22279113]

[3]. Mensah GA, Wei GS, Sorlie PD, Fine LJ, Rosenberg Y, Kaufmann PG, Mussolino ME, Hsu LL, Addou E, Engelgau MM, Gordon D, Decline in Cardiovascular Mortality: Possible Causes and Implications, Circ Res. 120 (2017) 366–380. 10.1161/CIRCRESAHA.116.309115. [PubMed: 28104770]

[4]. Bata IR, Gregor RD, Wolf HK, Brownell B, Trends in five-year survival of patients discharged after acute myocardial infarction, Canadian Journal of Cardiology. 22 (2006) 399–404. 10.1016/S0828-282X(06)70925-4. [PubMed: 16639475]

[5]. Hung J, Teng TK, Finn J, Knuiman M, Briffa T, Stewart S, Sanfilippo FM, Ridout S, Hobbs M, Trends From 1996 to 2007 in Incidence and Mortality Outcomes of Heart Failure After Acute Myocardial Infarction: A Population-Based Study of 20 812 Patients With First Acute Myocardial Infarction in Western Australia, Journal of the American Heart Association. 2 (n.d.) e000172. 10.1161/JAHA.113.000172.

[6]. Sulo G, Igland J, Vollset SE, Nygård O, Ebbing M, Sulo E, Egeland GM, Tell GS, Heart Failure Complicating Acute Myocardial Infarction; Burden and Timing of Occurrence: A Nation-wide Analysis Including 86 771 Patients From the Cardiovascular Disease in Norway (CVDNOR) Project, Journal of the American Heart Association. 5 (n.d.) e002667. 10.1161/JAHA.115.002667.

[7]. Blom AS, Mukherjee R, Pilla JJ, Lowry AS, Yarbrough WM, Mingoia JT, Hendrick JW, Stroud RE, McLean JE, Affuso J, Gorman RC, Gorman JH, Acker MA, Spinale FG, Cardiac Support Device Modifies Left Ventricular Geometry and Myocardial Structure After Myocardial Infarction, Circulation. 112 (2005) 1274–1283. 10.1161/CIRCULATIONAHA.104.499202. [PubMed: 16129812]

[8]. Khush KK, Menza R, Nguyen J, Zaroff JG, Goldstein BA, Donor Predictors of Allograft Use and Recipient Outcomes After Heart Transplantation, Circulation: Heart Failure. 6 (2013) 300–309. 10.1161/CIRCHEARTFAILURE.112.000165. [PubMed: 23392789]

[9]. Slaughter BV, Khurshid SS, Fisher OZ, Khademhosseini A, Peppas NA, Hydrogels in regenerative medicine, Adv Mater. 21 (2009) 3307–3329. 10.1002/adma.200802106. [PubMed: 20882499]

[10]. Delewi R, Hirsch A, Tijssen JG, Schächinger V, Wojakowski W, Roncalli J, Aakhus S, Erbs S, Assmus B, Tendera M, Goekmen Turan R, Corti R, Henry T, Lemarchand P, Lunde K, Cao F, Huikuri HV, Sürder D, Simari RD, Janssens S, Wollert KC, Plewka M, Grajek S, Traverse JH, Zijlstra F, Piek JJ, Impact of intracoronary bone marrow cell therapy on left ventricular function in the setting of ST-segment elevation myocardial infarction: a collaborative meta-analysis, European Heart Journal. 35 (2014) 989–998. 10.1093/eurheartj/eht372. [PubMed: 24026778]

[11]. Wollert KC, Drexler H, Clinical Applications of Stem Cells for the Heart, Circulation Research. 96 (2005) 151–163. 10.1161/01.RES.0000155333.69009.63. [PubMed: 15692093]

[12]. Li J, Hu S, Zhu D, Huang K, Mei X, López B de Juan Abad, Cheng K, All Roads Lead to Rome (the Heart): Cell Retention and Outcomes From Various Delivery Routes of Cell Therapy Products to the Heart, Journal of the American Heart Association. 10 (2021) e020402. 10.1161/JAHA.120.020402. [PubMed: 33821664]

[13]. Kieserman JM, Myers VD, Dubey P, Cheung JY, Feldman AM, Current Landscape of Heart Failure Gene Therapy, Journal of the American Heart Association. 8 (2019) e012239. 10.1161/JAHA.119.012239. [PubMed: 31070089]

[14]. Cannatà A, Ali H, Sinagra G, Giacca M, Gene Therapy for the Heart Lessons Learned and Future Perspectives, Circulation Research. 126 (2020) 1394–1414. 10.1161/CIRCRESAHA.120.315855. [PubMed: 32379579]

[15]. Segers VFM, Lee RT, Protein Therapeutics for Cardiac Regeneration after Myocardial Infarction, J. of Cardiovasc. Trans. Res. 3 (2010) 469–477. 10.1007/s12265-010-9207-5.

[16]. de J Rebouças S, Santos-Magalhães NS, Formiga FR, Cardiac Regeneration using Growth Factors: Advances and Challenges, Arq Bras Cardiol. 107 (2016) 271–275. 10.5935/abc.20160097. [PubMed: 27355588]

[17]. Fordyce CB, Roe MT, Ahmad T, Libby P, Borer JS, Hiatt WR, Bristow MR, Packer M, Wasserman SM, Braunstein N, Pitt B, DeMets DL, Cooper-Arnold K, Armstrong PW, Berkowitz SD, Scott R, Prats J, Galis ZS, Stockbridge N, Peterson ED, Califf RM, Cardiovascular Drug Development: Is it Dead or Just Hibernating?, Journal of the American College of Cardiology. 65 (2015) 1567–1582. 10.1016/j.jacc.2015.03.016. [PubMed: 25881939]

[18]. Wang X, Chen Y, Zhao Z, Meng Q, Yu Y, Sun J, Yang Z, Chen Y, Li J, Ma T, Liu H, Li Z, Yang J, Shen Z, Engineered Exosomes With Ischemic Myocardium-Targeting Peptide for Targeted Therapy in Myocardial Infarction, Journal of the American Heart Association. 7 (2018) e008737. 10.1161/JAHA.118.008737. [PubMed: 30371236]

[19]. Liu Z, Mikrani R, Zubair HM, Taleb A, Naveed M, Baig MMFA, Zhang Q, Li C, Habib M, Cui X, Sembatya KR, Lei H, Zhou X, Systemic and local delivery of mesenchymal stem cells for heart renovation: Challenges and innovations, European Journal of Pharmacology. 876 (2020) 173049. 10.1016/j.ejphar.2020.173049. [PubMed: 32142771]

[20]. van der Spoel TIG, Jansen of Lorkeers SJ, Agostoni P, van Belle E, Gyöngyösi M, Sluijter JPG, Cramer MJ, Doevendans PA, Chamuleau SAJ, Human relevance of pre-clinical studies in stem cell therapy: systematic review and meta-analysis of large animal models of ischaemic heart disease, Cardiovascular Research. 91 (2011) 649–658. 10.1093/cvr/cvr113. [PubMed: 21498423]

[21]. Bartunek J, Davison B, Sherman W, Povsic T, Henry TD, Gersh B, Metra M, Filippatos G, Hajjar R, Behfar A, Homsy C, Cotter G, Wijns W, Tendera M, Terzic A, Congestive Heart Failure Cardiopoietic Regenerative Therapy (CHART-1) trial design, European Journal of Heart Failure. 18 (2016) 160–168. 10.1002/ejhf.434. [PubMed: 26662998]

[22]. Sayed N, Liu C, Wu JC, Translation of Human-Induced Pluripotent Stem Cells: From Clinical Trial in a Dish to Precision Medicine, Journal of the American College of Cardiology. 67 (2016) 2161–2176. 10.1016/j.jacc.2016.01.083. [PubMed: 27151349]

[23]. Hofmann M, Wollert KC, Meyer GP, Menke A, Arseniev L, Hertenstein B, Ganser A, Knapp WH, Drexler H, Monitoring of Bone Marrow Cell Homing Into the Infarcted Human Myocardium, Circulation. 111 (2005) 2198–2202. 10.1161/01.CIR.0000163546.27639.AA. [PubMed: 15851598]

[24]. Blocklet D, Toungouz M, Berkenboom G, Lambermont M, Unger P, Preumont N, Stoupel E, Egrise D, Degaute J-P, Goldman M, Goldman S, Myocardial Homing of Nonmobilized Peripheral-Blood CD34+ Cells After Intracoronary Injection, STEM CELLS. 24 (2006) 333–336. 10.1634/stemcells.2005-0201. [PubMed: 16223854]

[25]. Müller-Ehmsen J, Whittaker P, Kloner RA, Dow JS, Sakoda T, Long TI, Laird PW, Kedes L, Survival and Development of Neonatal Rat Cardiomyocytes Transplanted into Adult Myocardium, Journal of Molecular and Cellular Cardiology. 34 (2002) 107–116. 10.1006/jmcc.2001.1491. [PubMed: 11851351]

[26]. Grossman PM, Han Z, Palasis M, Barry JJ, Lederman RJ, Incomplete retention after direct myocardial injection, Catheter Cardiovasc Interv. 55 (2002) 392–397. 10.1002/ccd.10136. [PubMed: 11870950]

[27]. Teng CJ, Luo J, Chiu RCJ, Shum-Tim D, Massive mechanical loss of microspheres with direct intramyocardial injection in the beating heart: Implications for cellular cardiomyoplasty, The Journal of Thoracic and Cardiovascular Surgery. 132 (2006) 628–632. 10.1016/j.jtcvs.2006.05.034. [PubMed: 16935119]

[28]. Liu J, Narsinh KH, Lan F, Wang L, Nguyen PK, Hu S, Lee A, Han L, Gong Y, Huang M, Nag D, Rosenberg J, Chouldechova A, Robbins RC, Wu JC, Early stem cell engraftment predicts late cardiac functional recovery: preclinical insights from molecular imaging, Circ Cardiovasc Imaging. 5 (2012) 481–490. 10.1161/CIRCIMAGING.111.969329. [PubMed: 22565608]

[29]. Malliaras K, Li T-S, Luthringer D, Terrovitis J, Cheng K, Chakravarty T, Galang G, Zhang Y, Schoenhoff F, Van Eyk J, Marbán L, Marbán E, Safety and Efficacy of Allogeneic Cell Therapy in Infarcted Rats Transplanted With Mismatched Cardiosphere-Derived Cells, Circulation. 125 (2012) 100–112. 10.1161/CIRCULATIONAHA.111.042598. [PubMed: 22086878]

[30]. Anderl JN, Robey TE, Stayton PS, Murry CE, Retention and biodistribution of microspheres injected into ischemic myocardium, Journal of Biomedical Materials Research Part A. 88A (2009) 704–710. 10.1002/jbm.a.31917.

[31]. Tayalia P, Mooney DJ, Controlled Growth Factor Delivery for Tissue Engineering, Advanced Materials. 21 (2009) 3269–3285. 10.1002/adma.200900241. [PubMed: 20882497]

[32]. Martens TP, Godier AFG, Parks JJ, Wan LQ, Koeckert MS, Eng GM, Hudson BI, Sherman W, Vunjak-Novakovic G, Percutaneous Cell Delivery Into the Heart Using Hydrogels Polymerizing In Situ, Cell Transplant. 18 (2009) 297–304. 10.3727/096368909788534915. [PubMed: 19558778]

[33]. van den Akker F, Feyen DAM, van den Hoogen P, van Laake LW, van Eeuwijk ECM, Hoefer I, Pasterkamp G, Chamuleau SAJ, Grundeman PF, Doevendans PA, Sluijter JPG, Intramyocardial stem cell injection: go(ne) with the flow, Eur Heart J. 38 (2017) 184–186. 10.1093/eurheartj/ehw056. [PubMed: 28158468]

[34]. Panda NC, Zuckerman ST, Mesubi OO, Rosenbaum DS, Penn MS, Donahue JK, Alsberg E, Laurita KR, Improved conduction and increased cell retention in healed MI using mesenchymal stem cells suspended in alginate hydrogel, J Interv Card Electrophysiol. 41 (2014) 117–127. 10.1007/s10840-014-9940-9. [PubMed: 25234602]

[35]. Wang H, Zhu D, Paul A, Cai L, Enejder A, Yang F, Heilshorn SC, Covalently Adaptable Elastin-Like Protein–Hyaluronic Acid (ELP–HA) Hybrid Hydrogels with Secondary Thermoresponsive Crosslinking for Injectable Stem Cell Delivery, Advanced Functional Materials. 27 (2017) 1605609. 10.1002/adfm.201605609. [PubMed: 33041740]

[36]. Zhu D, Wang H, Trinh P, Heilshorn SC, Yang F, Elastin-like protein-hyaluronic acid (ELP-HA) hydrogels with decoupled mechanical and biochemical cues for cartilage regeneration, Biomaterials. 127 (2017) 132–140. 10.1016/j.biomaterials.2017.02.010. [PubMed: 28268018]

[37]. Hunt DR, Klett KC, Mascharak S, Wang H, Gong D, Lou J, Li X, Cai PC, Suhar RA, Co JY, LeSavage BL, Foster AA, Guan Y, Amieva MR, Peltz G, Xia Y, Kuo CJ, Heilshorn SC, Engineered Matrices Enable the Culture of Human Patient-Derived Intestinal Organoids, Advanced Science. 8 (2021) 2004705. 10.1002/advs.202004705. [PubMed: 34026461]

[38]. LeSavage BL, Suhar NA, Madl CM, Heilshorn SC, Production of Elastin-like Protein Hydrogels for Encapsulation and Immunostaining of Cells in 3D, JoVE (Journal of Visualized Experiments). (2018) e57739. 10.3791/57739.

[39]. Tan H, Chu CR, Payne KA, Marra KG, Injectable in situ forming biodegradable chitosan-hyaluronic acid based hydrogels for cartilage tissue engineering, Biomaterials. 30 (2009) 2499–2506. 10.1016/j.biomaterials.2008.12.080. [PubMed: 19167750]

[40]. Chen Y-C, Su W-Y, Yang S-H, Gefen A, Lin F-H, In situ forming hydrogels composed of oxidized high molecular weight hyaluronic acid and gelatin for nucleus pulposus regeneration, Acta Biomater. 9 (2013) 5181–5193. 10.1016/j.actbio.2012.09.039. [PubMed: 23041783]

[41]. Krajina BA, Tropini C, Zhu A, DiGiacomo P, Sonnenburg JL, Heilshorn SC, Spakowitz AJ, Dynamic Light Scattering Microrheology Reveals Multiscale Viscoelasticity of Polymer Gels and Precious Biological Materials, ACS Cent. Sci. 3 (2017) 1294–1303. 10.1021/acscentsci.7b00449. [PubMed: 29296670]

[42]. Schindelin J, Arganda-Carreras I, Frise E, Kaynig V, Longair M, Pietzsch T, Preibisch S, Rueden C, Saalfeld S, Schmid B, Tinevez J-Y, White DJ, Hartenstein V, Eliceiri K, Tomancak P, Cardona A, Fiji: an open-source platform for biological-image analysis, Nature Methods. 9 (2012) 676–682. 10.1038/nmeth.2019. [PubMed: 22743772]

[43]. Sbalzarini IF, Koumoutsakos P, Feature point tracking and trajectory analysis for video imaging in cell biology, J Struct Biol. 151 (2005) 182–195. 10.1016/j.jsb.2005.06.002. [PubMed: 16043363]

[44]. Mitsutake Y, Pyun WB, Rouy D, Foo CWP, Stertzer SH, Altman P, Ikeno F, Improvement of Local Cell Delivery Using Helix Transendocardial Delivery Catheter in a Porcine Heart, International Heart Journal. 58 (2017) 435–440. 10.1536/ihj.16-179. [PubMed: 28539564]

[45]. Crisostomo V, Baez C, Abad JL, Sanchez B, Alvarez V, Rosado R, Gómez-Mauricio G, Gheysens O, Blanco-Blazquez V, Blazquez R, Torán JL, Casado JG, Aguilar S, Janssens S, Sánchez-Margallo FM, Rodriguez-Borlado L, Bernad A, Palacios I, Dose-dependent improvement of cardiac function in a swine model of acute myocardial infarction after intracoronary administration of allogeneic heart-derived cells, Stem Cell Research & Therapy. 10 (2019) 152. 10.1186/s13287-019-1237-6. [PubMed: 31151405]

[46]. Collantes M, Pelacho B, García-Velloso MJ, Gavira JJ, Abizanda G, Palacios I, Rodriguez-Borlado L, Álvarez V, Prieto E, Ecay M, Larequi E, Peñuelas I, Prósper F, Non-invasive in vivo imaging of cardiac stem/progenitor cell biodistribution and retention after intracoronary and intramyocardial delivery in a swine model of chronic ischemia reperfusion injury, J Transl Med. 15 (2017) 56. 10.1186/s12967-017-1157-0. [PubMed: 28288654]

[47]. Vrtovec B, Poglajen G, Lezaic L, Sever M, Socan A, Domanovic D, Cernelc P, Torre-Amione G, Haddad F, Wu JC, Comparison of Transendocardial and Intracoronary CD34+ Cell Transplantation in Patients With Nonischemic Dilated Cardiomyopathy, Circulation. 128 (2013) S42–S49. 10.1161/CIRCULATIONAHA.112.000230. [PubMed: 24030420]

[48]. Silva SA, Sousa ALS, Haddad AF, Azevedo JC, Soares VE, Peixoto CM, Soares AJS, Issa AFC, Felipe LRV, Branco RVC, Addad JA, Moreira RC, Tuche FAA, Mesquita CT, Drumond CCO,

Junior AO, Rochitte CE, Luz JHM, Rabischoffisky A, Nogueira FB, Vieira RBC, Junior HS, Borojevic R, Dohmann HFR, Autologous bone-marrow mononuclear cell transplantation after acute myocardial infarction: comparison of two delivery techniques, Cell Transplant. 18 (2009) 343–352. 10.3727/096368909788534951. [PubMed: 19558782]

[49]. Musialek P, Tekieli L, Kostkiewicz M, Majka M, Szot W, Walter Z, Zebzda A, Pieniazek P, Kadzielski A, Banys RP, Olszowska M, Pasowicz M, Zmudka K, Tracz W, Randomized transcoronary delivery of CD34+ cells with perfusion versus stop-flow method in patients with recent myocardial infarction: Early cardiac retention of 99mTc-labeled cells activity, J. Nucl. Cardiol. 18 (2011) 104–116. 10.1007/s12350-010-9326-z. [PubMed: 21161463]

[50]. Yang H, Qin X, Wang H, Zhao X, Liu Y, Wo H-T, Liu C, Nishiga M, Chen H, Ge J, Sayed N, Abilez OJ, Ding D, Heilshorn SC, Li K, An in Vivo miRNA Delivery System for Restoring Infarcted Myocardium, ACS Nano. 13 (2019) 9880–9894. 10.1021/acsnano.9b03343. [PubMed: 31149806]

[51]. Pandit AH, Mazumdar N, Ahmad S, Periodate oxidized hyaluronic acid-based hydrogel scaffolds for tissue engineering applications, International Journal of Biological Macromolecules. 137 (2019) 853–869. 10.1016/j.ijbiomac.2019.07.014. [PubMed: 31284008]

[52]. Muhammad M, Willems C, Rodríguez-Fernández J, Gallego-Ferrer G, Groth T, Synthesis and Characterization of Oxidized Polysaccharides for In Situ Forming Hydrogels, Biomolecules. 10 (2020) 1185. 10.3390/biom10081185.

[53]. McKinnon DD, Domaille DW, Cha JN, Anseth KS, Biophysically Defined and Cytocompatible Covalently Adaptable Networks as Viscoelastic 3D Cell Culture Systems, Adv Mater. 26 (2014) 865–872. 10.1002/adma.201303680. [PubMed: 24127293]

[54]. Li L, Wang N, Jin X, Deng R, Nie S, Sun L, Wu Q, Wei Y, Gong C, Biodegradable and injectable in situ cross-linking chitosan-hyaluronic acid based hydrogels for postoperative adhesion prevention, Biomaterials. 35 (2014) 3903–3917. 10.1016/j.biomaterials.2014.01.050. [PubMed: 24507411]

[55]. Wang LL, Highley CB, Yeh Y-C, Galarraga JH, Uman S, Burdick JA, Three-dimensional extrusion bioprinting of single- and double-network hydrogels containing dynamic covalent crosslinks, Journal of Biomedical Materials Research Part A. 106 (2018) 865–875. 10.1002/jbm.a.36323. [PubMed: 29314616]

[56]. Tang S, Ma H, Tu H, Wang H, Lin P, Anseth KS, Adaptable Fast Relaxing Boronate-Based Hydrogels for Probing Cell–Matrix Interactions, Adv Sci (Weinh). 5 (2018) 1800638. 10.1002/advs.201800638. [PubMed: 30250802]

[57]. Straley KS, Heilshorn SC, Design and Adsorption of Modular Engineered Proteins to Prepare Customized, Neuron-Compatible Coatings, Front Neuroengineering. 2 (2009) 9. 10.3389/neuro.16.009.2009.

[58]. Olsen BD, Kornfield JA, Tirrell DA, Yielding Behavior in Injectable Hydrogels from Telechelic Proteins, Macromolecules. 43 (2010) 9094–9099. 10.1021/ma101434a. [PubMed: 21221427]

[59]. Yan C, Altunbas A, Yucel T, Nagarkar RP, Schneider JP, Pochan DJ, Injectable solid hydrogel: mechanism of shear-thinning and immediate recovery of injectable β-hairpin peptide hydrogels, Soft Matter. 6 (2010) 5143–5156. 10.1039/C0SM00642D. [PubMed: 21566690]

[60]. Munson B, Young D, Okiishi T, Section 8.4, in: Fundamentals of Fluid Mechanics, 5th ed., Wiley, Hoboken, NJ, 2018.

[61]. Riley L, Schirmer L, Segura T, Granular hydrogels: emergent properties of jammed hydrogel microparticles and their applications in tissue repair and regeneration, Curr Opin Biotechnol. 60 (2019) 1–8. 10.1016/j.copbio.2018.11.001. [PubMed: 30481603]

[62]. Qazi TH, Burdick JA, Granular hydrogels for endogenous tissue repair, Biomaterials and Biosystems. 1 (2021) 100008. 10.1016/j.bbiosy.2021.100008.

[63]. Ou L, Li W, Zhang Y, Wang W, Liu J, Sorg H, Furlani D, Gäbel R, Mark P, Klopsch C, Wang L, Lützow K, Lendlein A, Wagner K, Klee D, Liebold A, Li R-K, Kong D, Steinhoff G, Ma N, Intracardiac injection of matrigel induces stem cell recruitment and improves cardiac functions in a rat myocardial infarction model, J Cell Mol Med. 15 (2011) 1310–1318. 10.1111/j.1582-4934.2010.01086.x. [PubMed: 20477905]

[64]. Marquardt LM, Heilshorn SC, Design of Injectable Materials to Improve Stem Cell Transplantation, Curr Stem Cell Rep. 2 (2016) 207–220. 10.1007/s40778-016-0058-0.

[65]. Breckenridge RA, Chapter 7 - Animal Models of Myocardial Disease, in: Conn PM(Ed.), Animal Models for the Study of Human Disease, Academic Press, Boston, 2013: pp. 145–171. 10.1016/B978-0-12-415894-8.00007-5.

[66]. Hou D, Youssef EA-S, Brinton TJ, Zhang P, Rogers P, Price ET, Yeung AC, Johnstone BH, Yock PG, March KL, Radiolabeled cell distribution after intramyocardial, intracoronary, and interstitial retrograde coronary venous delivery: implications for current clinical trials, Circulation. 112 (2005) I150–156. 10.1161/CIRCULATIONAHA.104.526749. [PubMed: 16159808]

[67]. Martens A, Rojas SV, Baraki H, Rathert C, Schecker N, Hernandez SR, Schwanke K, Zweigerdt R, Martin U, Saito S, Haverich A, Kutschka I, Macroscopic Fluorescence Imaging: A Novel Technique to Monitor Retention and Distribution of Injected Microspheres in an Experimental Model of Ischemic Heart Failure, PLOS ONE. 9 (2014) e101775. 10.1371/journal.pone.0101775. [PubMed: 25089764]

[68]. Stern R, Asari AA, Sugahara KN, Hyaluronan fragments: An information-rich system, European Journal of Cell Biology. 85 (2006) 699–715. 10.1016/j.ejcb.2006.05.009. [PubMed: 16822580]

[69]. Papanastasopoulou C, Papastamataki M, Karampatsis P, Anagnostopoulou E, Papassotiriou I, Sitaras N, Cardiovascular Risk and Serum Hyaluronic Acid: A Preliminary Study in a Healthy Population of Low/Intermediate Risk, Journal of Clinical Laboratory Analysis. 31 (2017) e22010. 10.1002/jcla.22010.

[70]. Yoon SJ, Fang YH, Lim CH, Kim BS, Son HS, Park Y, Sun K, Regeneration of ischemic heart using hyaluronic acid-based injectable hydrogel, J Biomed Mater Res B Appl Biomater. 91 (2009) 163–171. 10.1002/jbm.b.31386. [PubMed: 19399850]

[71]. Chaudhuri O, Gu L, Klumpers D, Darnell M, Bencherif SA, Weaver JC, Huebsch N, Lee H, Lippens E, Duda GN, Mooney DJ, Hydrogels with tunable stress relaxation regulate stem cell fate and activity, Nature Mater. 15 (2016) 326–334. 10.1038/nmat4489. [PubMed: 26618884]

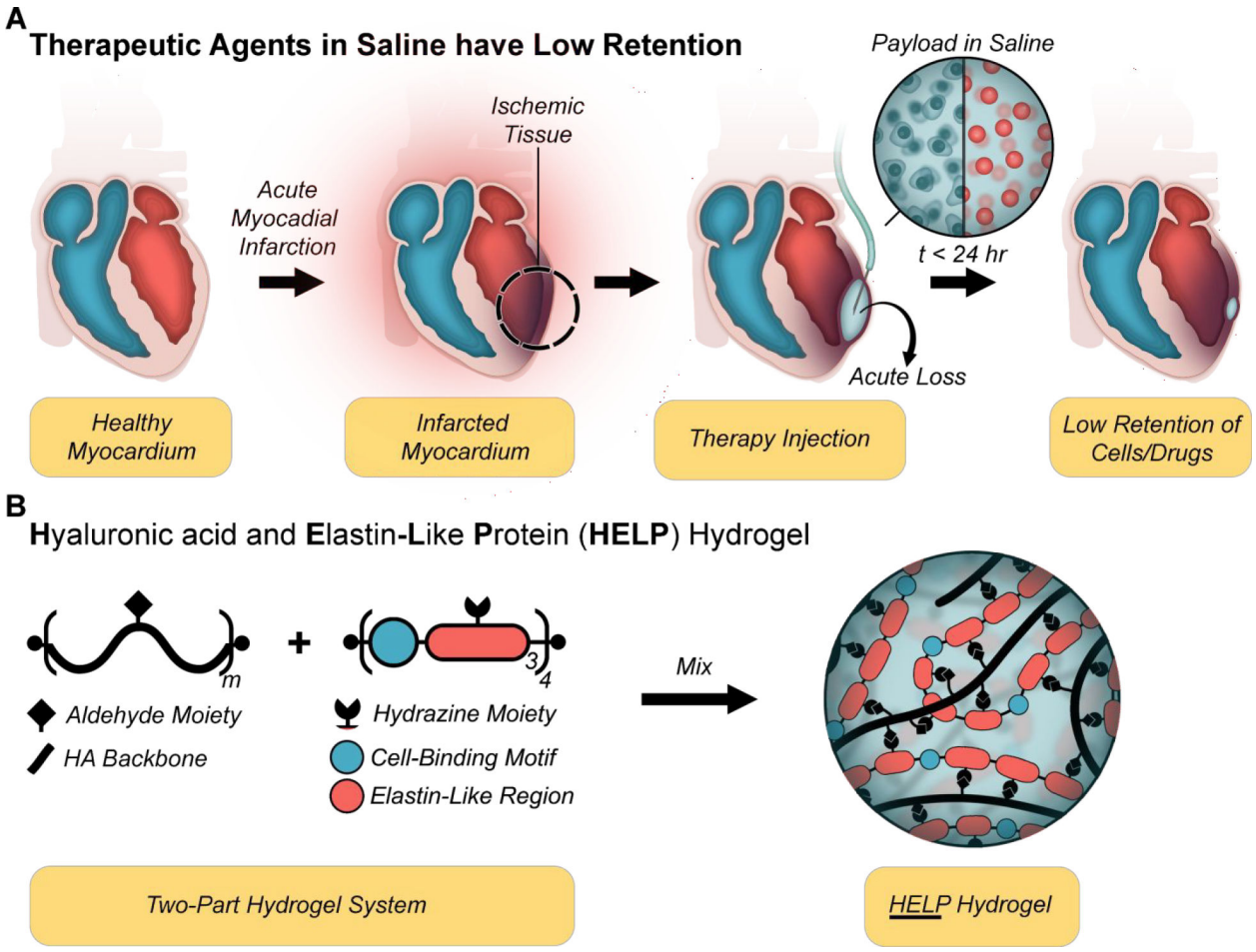

Figure 1. Injectable hydrogel strategy to improve myocardium retention:

(A) Schematic of acute reflux following injection of therapeutic agents (cells (blue) and/or drug-loaded particles (red)) suspended in saline. (B) A two-part hydrogel (termed HELP, hyaluronan and elastin-like protein) is designed to improve the retention of therapeutic agents injected into the myocardium. Hyaluronan (also called hyaluronic acid; HA) is modified via oxidation or bio-conjugation reaction to display aldehydes, while the recombinant elastin-like protein (ELP) presents hydrazine moieties allowing formation of hydrazone bonds upon mixing.

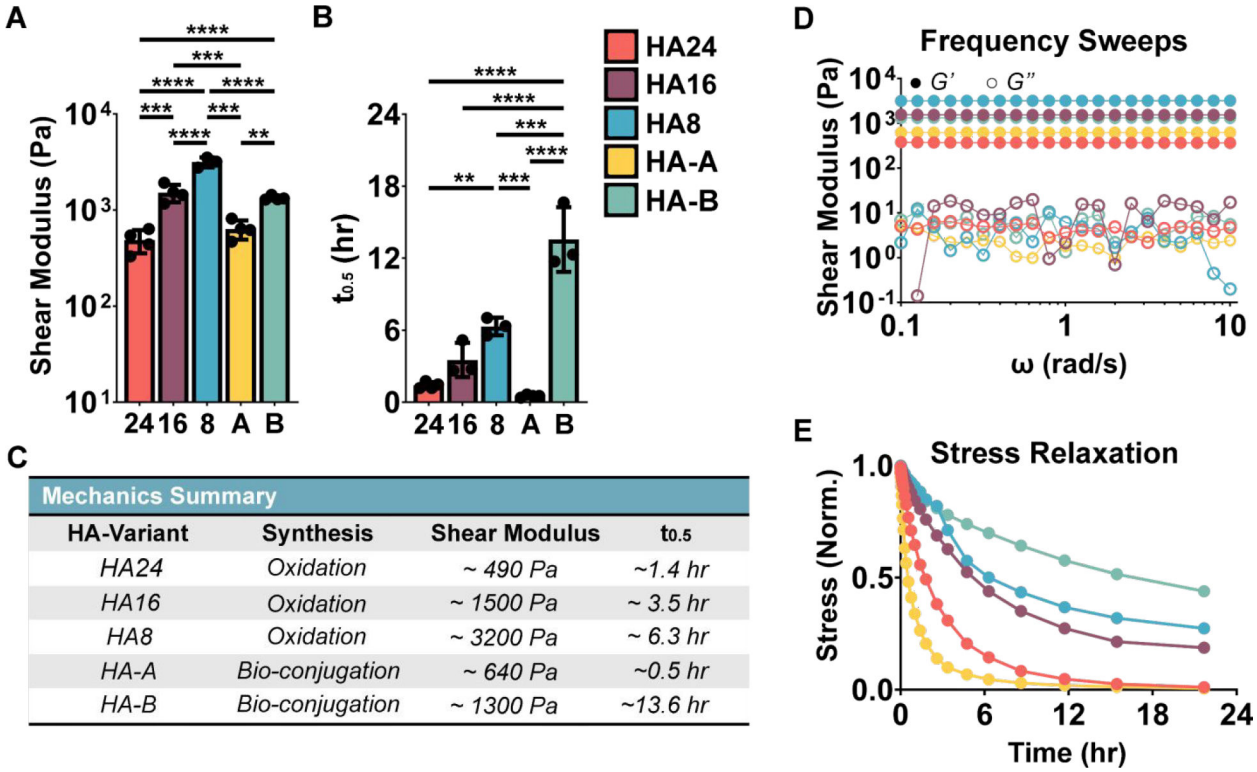

Mechanics Summary

HA-Variant	Synthesis	Shear Modulus	$t_{0.5}$
HA24	*Oxidation*	*~ 490 Pa*	*~1.4 hr*
HA16	*Oxidation*	*~ 1500 Pa*	*~ 3.5 hr*
HA8	*Oxidation*	*~ 3200 Pa*	*~ 6.3 hr*
HA-A	*Bio-conjugation*	*~ 640 Pa*	*~0.5 hr*
HA-B	*Bio-conjugation*	*~ 1300 Pa*	*~13.6 hr*

Figure 2. Hyaluronic acid and Elastin-Like Protein (HELP) Hydrogel Mechanics:

(A) Summary frequency sweep and (B) stress relaxation data. (C) Average values of maximum storage moduli and stress relaxation time ($t_{0.5}$) for each gel variant are summarized. Representative (D) frequency sweep and I normalized stress-relaxation curves are additionally presented for reference. The HELP systems presented here form robust gels with a shear modulus range from ~490 Pa to ~3200 Pa and stress relaxation ($t_{0.5}$) times from ~0.51 hr. to 13.6 hr. One-way ANOVA, $\alpha = 0.05$, post-hoc Tukey test, ** $p < 0.01$, *** $p < 0.001$, **** $p < 0.0001$.

A

Injection Criterion
1. Injectable after complete gelation.
2. Injectable with one hand through a 30-G needle.
3. Must have no “burst” injection.

B

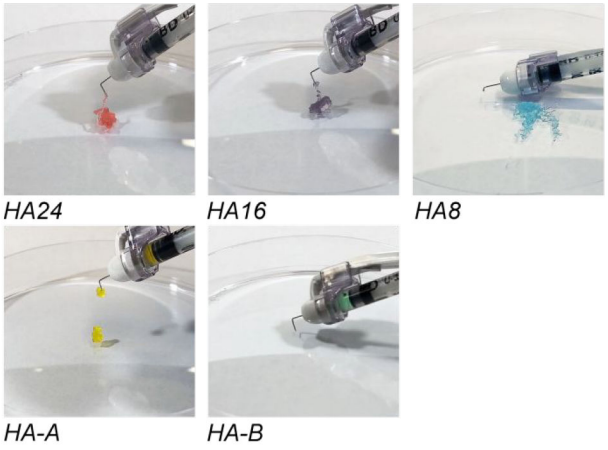

C

Injection Scording			
HA-Variant	1	2	3
HA24	✓	✓	✓
HA16	✓	✓	✓
HA8	✓	✗	✗
HA-A	✓	✗	✗
HA-B	✗	-	-

Figure 3. Hydrogel Injectability Screening and Qualitative Assessment:

The qualitative injectability of HELP gels were tested by injecting each formulation following complete crosslinking (30 min) through a hooked, 30-G insulin needle. (A) Injectability criteria included: (1) ability to be injectable after complete gelation, with one or two hands, (2) injectable with one hand, and (3) no evidence of a sudden burst injection. (B) Qualitative stills taken from recordings of each injection. Note: brightness has been artificially increased for ease of viewing. Additionally, each gel has been dyed with food coloring to match their prescribed color scheme as presented in this manuscript. (C) Table summarizing the qualitative assessment, where a check mark (✓) and a cross (x) signify satisfying or failing a criterion, respectively.

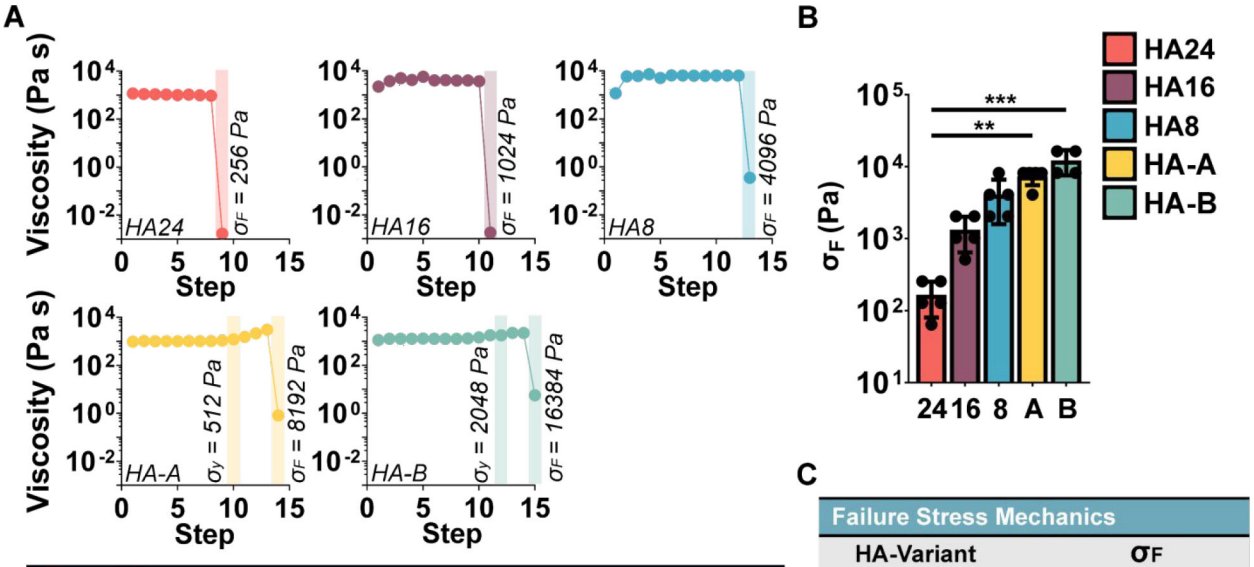

C

Stress Steps									
Step	1	2	3	4	5	6	7	8	9
Stress (Pa)	1	2	4	8	16	32	64	128	256
Step	10	11	12	13	14	15			
Stress (Pa)	512	1024	2048	4096	8182	16384			

Failure Stress Mechanics	
HA-Variant	σF
HA24	~ 170 Pa
HA16	~ 1300 Pa
HA8	~ 4100 Pa
HA-A	~ 7600 Pa
HA-B	~ 12000 Pa

Figure 4. Hydrogel Fracture Stress:

To quantify fracture stress (σ^F) we measured the gel apparent viscosity ($\eta = \sigma / \gamma$) as a function of stress, with increasing stress intervals. The gel fracture stress (σ^F) was defined as the stress step that led to an abrupt decrease in viscosity. (A) Representative measurements of apparent viscosity at increasing stress step intervals. σ_F denotes failure stress; σ_y denotes yield stress. (B) Average fracture stress for each HELP gel formulation (n = 4 – 5). (C) Tabulated fracture stress values demonstrate that the two injectable formulations identified previously (HA24 and HA16, designated with a dotted outline) have the lowest fracture stress. Kruskal-Wallis test $\alpha = 0.05$, with post-hoc Dunn's test, ** $p < 0.01$, *** $p < 0.001$.

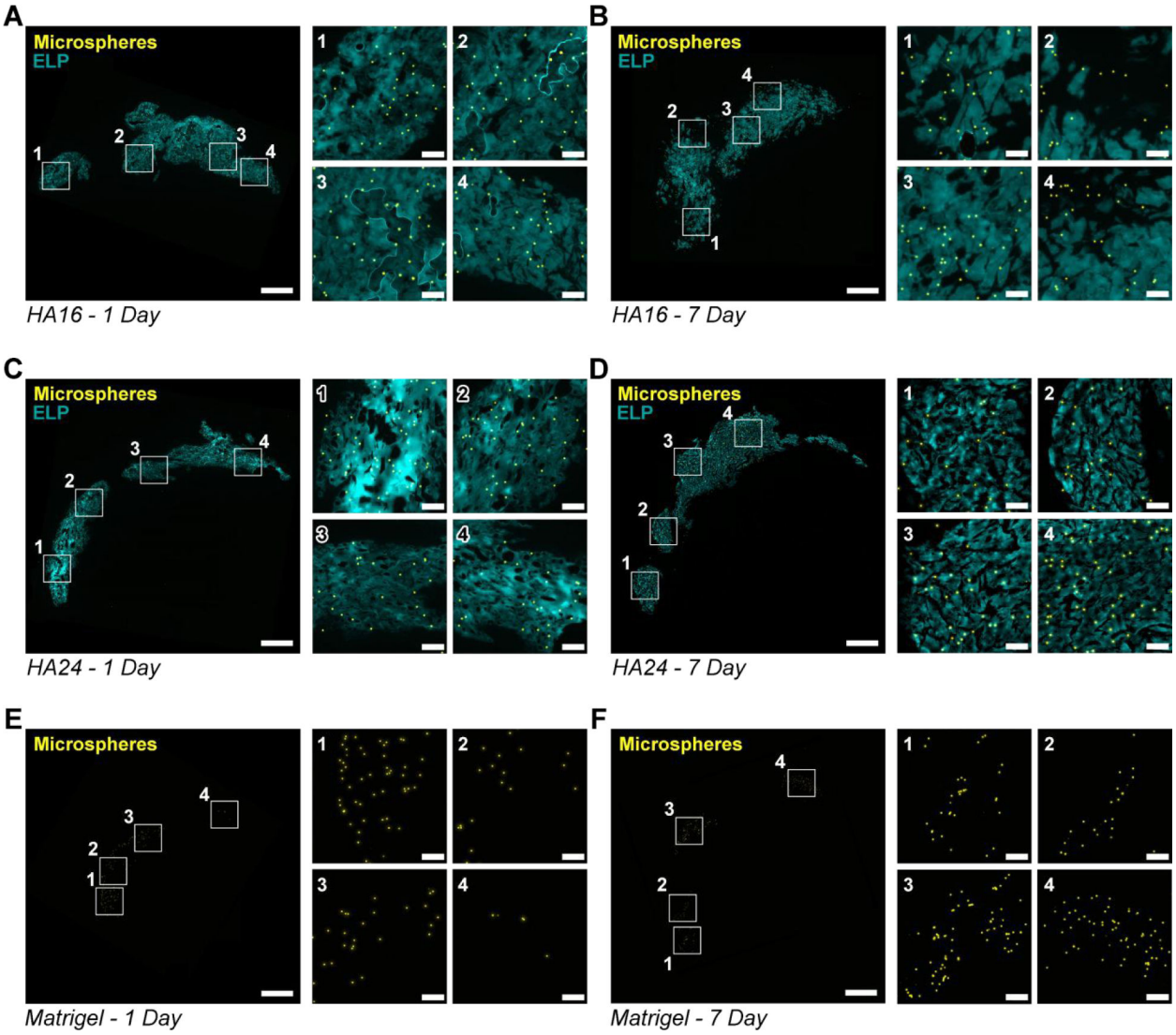

Figure 5. Gel-mediated cargo retention in myocardium:

Representative fluorescence images (elastin-like protein (ELP), cyan; microspheres, yellow), of tissue sections collected from hearts at 1 day and 7 days post-injection with HA16 (A, B), HA24 (C, D) and Matrigel (E, F). For ease of viewing, a single low-magnification and four high-magnification (indicated by a white outline and corresponding number) fields of view are shown. Scale bar on low and high magnification images are 1-mm and 100-μm, respectively.

A

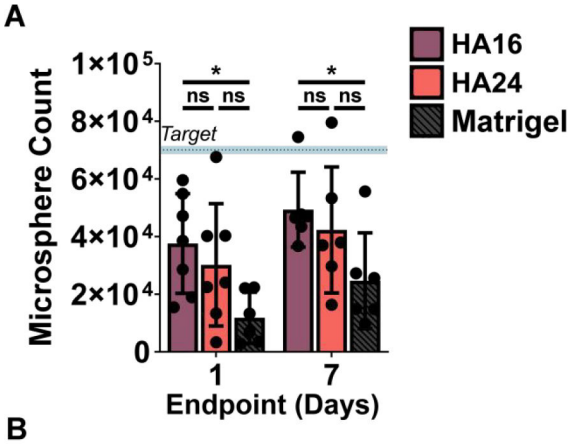

B

Average Microsphere Count				
Hydrogel	1 Day	n	7 Day	n
HA16	*~ 37900*	*7*	*~ 49300*	*6*
HA24	*~ 30200*	*7*	*~ 42300*	*6*
Matrigel	*~ 11800*	*6*	*~ 24700*	*6*

C

Microsphere Retention (% Target)				
Hydrogel	1 Day	n	7 Day	n
HA16	*53.6% ± 24.6%*	*7*	*70.4% ± 18.5%*	*6*
HA24	*43.1% ± 30.3%*	*7*	*60.4% - 31.2%*	*6*
Matrigel	*16.9% ± 12.6%*	*6*	*35.2% - 23.7%*	*6*

Figure 6. Quantified microsphere and hydrogel retention:

(A) HA16 significantly increased cargo retention over Matrigel at both time points. Summary of the approximate bead count and percent retention have been provided for reference in (B) and (C), respectively. One-way ANOVA, $\alpha = 0.05$, post-hoc Tukey test, * $p < 0.05$, ns = not significant.

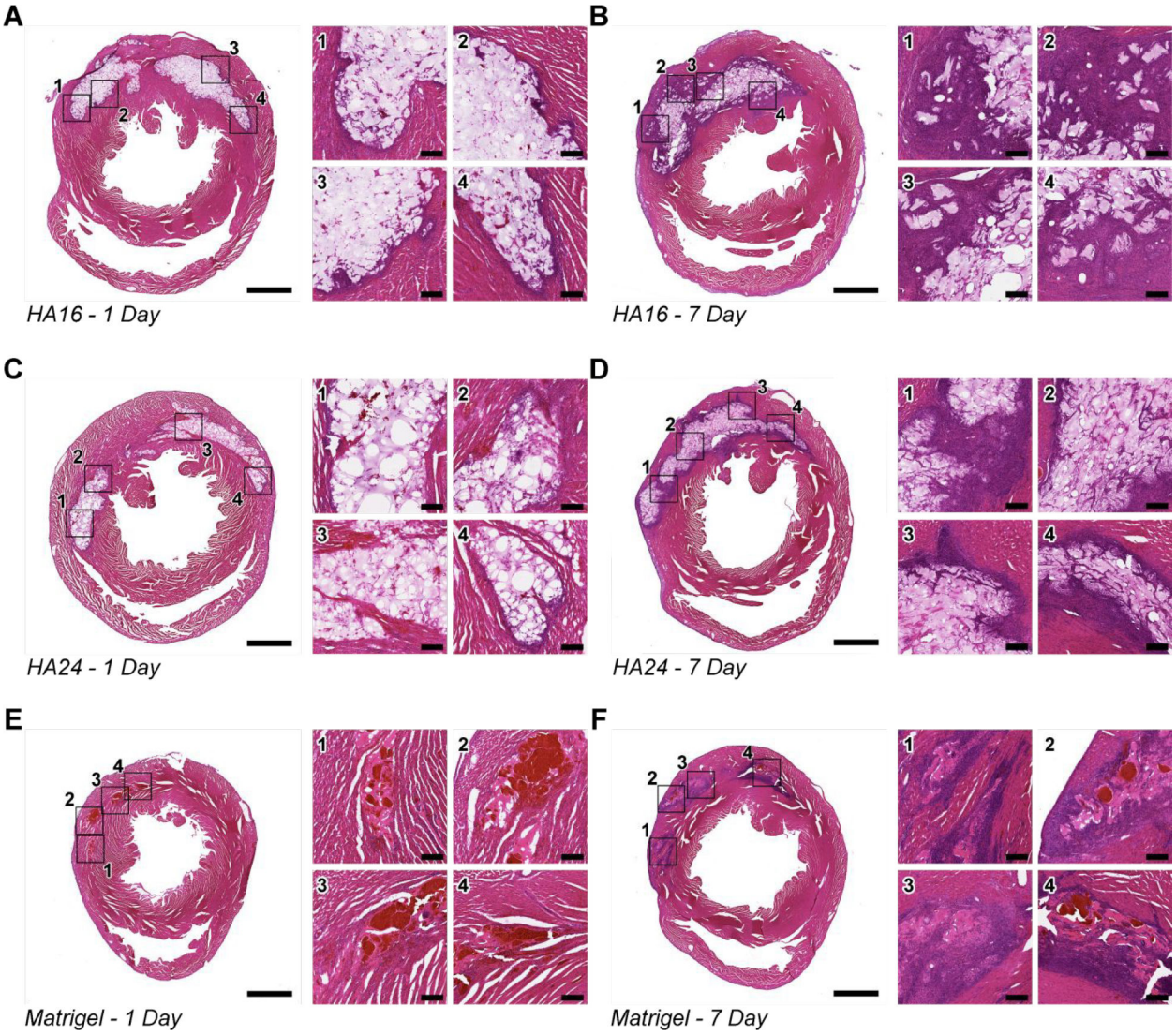

Figure 7. Hematoxylin and Eosin Staining of Representative Tissue Sections:

Representative Hematoxylin & Eosin (H&E) stains of tissue sections from hearts 1-day (left) and 7 days (right) after injection with HA16 (A, B), HA24 (C, D) and Matrigel (E, F). For ease of viewing, a single low-magnification and four high-magnification (indicated by a black outline and corresponding numbers) have been generated. Of note, in all cases, there is an increase in cell-infiltration between Day 1 (A, C, E) and Day 7 (B, D, F) post-injection, indicated by the increase of cell nuclei (purple) in and around the implanted hydrogels. In addition, while there does not appear to be a qualitative difference in gel area between HA16 and HA24 both appear to have a greater gel cross-section than Matrigel. Note: scale bar on low magnification images represents 2-mm, scale bar on high-magnification images represents 200-μm.

Table 1.

In vivo Test Groups: Following our injection study, both the HA16 and HA24 were selected for in vivo testing along with Matrigel as a control. For testing, 38, 10-week-old, Sprague Dawley rats were divided into sex-matched cohorts: 1 and 2, which were allocated to endpoint analyses at day 1 and day 7 post-injection, respectively.

Test Groups				
	Cohort 1		Cohort 2	
Hydrogel	**n**	**Endpoint**	**n**	**Endpoint**
HA16	*4♀ 3♂*	*1 Day*	*3♀ 3♂*	*7 Day*
HA24	*3♀ 4♂*	*1 Day*	*3♀ 3♂*	*7 Day*
Matrigel	*3♀ 3♂*	*1 Day*	*3♀ 3♂*	*7 Day*